

# Analytic One-loop Scattering Waveform in General Relativity

Giacomo Brunello<sup>a,b,c,\*</sup>, Stefano De Angelis<sup>a,†</sup> and David A. Kosower<sup>a,‡</sup>

<sup>a</sup>*Institut de Physique Théorique, CEA, CNRS, Université Paris-Saclay, F-91191 Gif-sur-Yvette cedex, France*

<sup>b</sup>*Dipartimento di Fisica e Astronomia, Università degli Studi di Padova  
and INFN Sezione di Padova, Via Marzolo 8, I-35131 Padova, Italy. and*

<sup>c</sup>*Scuola Normale Superiore, Piazza dei Cavalieri 7, 56126, Pisa,*

*Italy and INFN Sezione di Pisa, Largo Pontecorvo 3, 56127 Pisa, Italy*

(Dated: November 10, 2025)

Leveraging the computational framework presented in reference [1], we evaluate the analytic scattering waveform in General Relativity to second order,  $G^3 M^3 / r b^2$  and to all orders in velocity. This new representation of the next-to-leading order waveform is well-suited for numerical evaluation. Integrating the [modulus square of the] waveform over the angles on the celestial sphere, we also compute the power spectrum of the radiation to order  $G^4$  numerically.

## I. INTRODUCTION

The emerging precision era in gravitational-wave (GW) physics demands a deeper theoretical understanding of gravitational waveforms in order to produce more accurate templates for matched-filtering analyses. Although the so-called ‘Multipolar Post-Minkowskian’ (MPM) formalism has been successful in describing gravitational-wave emission from a variety of sources analytically [2–4], recent years’ developments originating in quantum field theory have offered a new approach and new tools for attacking the relativistic two-body problem. These include approaches based on effective field theory (EFT) [5], quantum scattering amplitudes, and world-line formalisms. The new approaches have driven progress in both the traditional post-Newtonian (PN) and ordinary relativistic perturbative predictions. In the PN approach, EFT methods [5–8], combined with multi-loop techniques [9], have allowed calculations to reach 4PN [10–12] and even 5PN [13–15]. In relativistic perturbation theory, the connection with scattering amplitudes was understood long ago [16], but only recently has a path to applying scattering amplitudes to gravitational calculations been suggested [17, 18] and carried out. The calculation of the  $\mathcal{O}(G^3)$  corrections to the gravitational Hamiltonian using scattering amplitudes [19, 20] was the opening shot to a flood of research activity. These corrections in turn yielded the corrections to the emitted gravitational energy. The development of methods based on scattering amplitudes made possible the calculation of the  $\mathcal{O}(G^4)$  corrections [21–27], methods based on a world-line quantum field theory (WQFT) approach [28, 29] then yielded the  $\mathcal{O}(G^5)$  corrections [30–36]. Most recently, several groups have computed the  $\mathcal{O}(G^6)$  corrections at the first self-force order [37–40]. These corrections to the gravitational Hamiltonian again have led to substantial improvement in the perturbative

predictions near merger as compared with (expensive) predictions from numerical relativity [41, 42]. The world-line methods also allowed the direct computation of the scattering waveform at lowest order for spinless particles [43, 44]. These methods made possible the computation of the waveform at tree-level for spinless particles within the worldline formalism and including spin corrections [45–48]. An earlier formalism (observables-based *aka* KMOC) [49, 50] links the usual quantum scattering amplitudes to classical observables.

In this article, we use the KMOC formalism to obtain an analytic result for the scattering gravitational waveform in impact parameter space. We compute the waveform arising from the scattering of two celestial objects to next-to-leading order ( $\mathcal{O}(G^3)$ ). The waveform in momentum space was obtained previously [51–55]; however, the physical waveform, as measured by GW observatories, is related to this result only through a Fourier transform (FT). The FT is a non-trivial step, even when done numerically, as emphasized by several authors [51, 52, 55].

In this article we extend the strategy introduced by two of the authors [1] to gravitational systems. Our central object is the frequency-domain waveform, to which we apply scattering-amplitude techniques directly. We consider the Fourier transform on the same footing as the loop integrations, and apply reduction techniques to the combined integrals.

We apply unitarity-based techniques for integrand reconstruction [56–61] uniformly to both the loop and Fourier momenta [1]. We simplify the generation of integrands by performing a classical expansion at the integrand level, using a heavy mass expansion [26, 62]. We also extend integration-by-parts (IBP) identities [63–70] to include the exponential factor in the Fourier transform [1, 71–74]. We then use IBPs in a standard fashion to reduce the integrated form of the amplitude to a sum of master integrals (MIs) alongside their coefficients.

We are able to express the waveform using a novel basis of 28 functions. Remarkably, while our computations are for spinless compact objects, the same basis suffices to express waveforms of spinning compact objects.

*Notation* As is standard in scattering amplitudes, we work in the mostly minus signature (+, −, −, −), with rel-

\* giacomo.brunello@sns.it

† stefano.de-angelis@ipht.fr

‡ david.kosower@ipht.fr

ativistic units  $c = 1$ . As usual, we define the coupling  $\kappa := \sqrt{32\pi G}$ , where  $G$  is Newton's constant. We adopt a  $\pi$ -absorbing *hat* notation [49] for the integral measure,

$$\hat{d}^m q := \frac{d^m q}{(2\pi)^m}, \quad (\text{I.1})$$

and for delta functions,

$$\hat{\delta}^{(m)}(\cdot) := (2\pi)^m \delta^{(m)}(\cdot). \quad (\text{I.2})$$

We also abbreviate loop-integral ( $\ell$ ) and combined Fourier- ( $q$ ) and loop-integral measures, defining,

$$\begin{aligned} \int_{\hat{\ell}} &:= e^{\epsilon\gamma_E} \int \hat{d}^D \ell, \\ \int_{\hat{q}, \hat{\ell}} &:= e^{\epsilon\gamma_E} \int \hat{d}^D q \hat{d}^D \ell, \end{aligned} \quad (\text{I.3})$$

where the exponential factor is intended to remove explicit appearances of  $\gamma_E$  in finite parts of integrals. The amplitudes have graviton momenta outgoing. For in- and out-states, scalar momenta are taken to be incoming and outgoing, respectively. We take  $\hbar = 1$  in the initial quantum expressions, and leave implicit its restoration and the taking of  $\hbar \rightarrow 0$  to obtain the classical limit. We leave the change from massive momenta to wavenumbers in the classical limit implicit as well.

## II. FRAMEWORK

Following the KMOC approach [49, 50, 75], classical observables such as the gravitational waveform are defined as the classical limits of quantum observables. The latter are given by the difference between the expectation value of a quantum operator  $\mathcal{O}$  in the final  $|\psi\rangle_{\text{out}}$  and initial  $|\psi\rangle_{\text{in}}$  states. The final states are given by the unitarity evolution of the initial states via the  $S$ -matrix,

$$|\psi\rangle_{\text{out}} = S |\psi\rangle_{\text{in}}. \quad (\text{II.1})$$

The  $S$ -matrix can be expressed in terms of the transfer matrix  $T$  as:

$$S = 1 + iT. \quad (\text{II.2})$$

In our work we will define scattering amplitudes  $\mathcal{M}(i \rightarrow f)$  as the matrix elements of  $T$ :

$$\mathcal{M}(i \rightarrow f) \hat{\delta}^D(k_i - k_f) = \langle f | T | i \rangle. \quad (\text{II.3})$$

Thus, following the definition of (II.1), a generic observable is written as:

$$\langle \Delta \mathcal{O} \rangle = \langle \mathcal{O} \rangle_{\text{out}} - \langle \mathcal{O} \rangle_{\text{in}} = {}_{\text{in}} \langle \psi | S^\dagger [\mathcal{O}, S] | \psi \rangle_{\text{in}}. \quad (\text{II.4})$$

Equivalently, we could compute expectation values in quantum field theory (QFT) using the Schwinger–Keldysh formalism [76, 77]. This formalism is equivalent to the KMOC approach based on scattering amplitude

computations, and is more commonly used within the WQFT approach [78, 79]. The two formalisms are expected to produce the same results. Indeed, we may observe that several terms in the KMOC formulation combine to produce the retarded propagators characteristic of Schwinger–Keldysh approach [54].

In this article, we will use the KMOC approach to compute the radiation waveform emerging from gravitational scattering of a two-body system. We build the appropriate initial state out of two-particle plane-wave states  $|p_1, p_2\rangle_{\text{in}}$ . We take a superposition given by on-shell wavefunctions  $\phi_i(p_i)$ ,

$$|\psi\rangle_{\text{in}} = \int \prod_{i=1}^2 d\Phi(p_i) \phi_i(p_i) e^{ib_i \cdot p_i} |p_1, p_2\rangle_{\text{in}}, \quad (\text{II.5})$$

where  $d\Phi(p_i)$  is the Lorentz-invariant on-shell phase-space (LIPS) measure, and the vectors  $b_{1,2}^\mu$  encode the transverse separations of the two wavepackets with respect to the chosen origin. The impact parameter is the difference of the separation vectors,  $b^\mu = b_1^\mu - b_2^\mu$ ; it is space-like. Strongly localizing the wavefunctions  $\phi(p_i)$  around a classical value of the momenta [49] will take the classical limit of the observable, suppressing quantum corrections.

The gravitational waveform is given by the expectation value of the gravitational field operator in the far future as a function of the (retarded) time and the angles on the celestial sphere. In our case, we may choose,

$$\mathcal{O}_\mathcal{W} = \kappa \varepsilon_\lambda^{\mu\nu} h_{\mu\nu}, \quad (\text{II.6})$$

where  $\lambda$  denotes the helicity configuration of the waves which we are interested in observing, and  $h_{\mu\nu}$  is the quantum operator corresponding to linearized deviations from a background metric, linearized metric field ( $g_{\mu\nu} = \eta_{\mu\nu} + h_{\mu\nu}^{\text{cl}}$ ). As we approach an infinite distance from the source, this is equivalent to the Riemann (and also Weyl) tensor observables considered in Ref. [50], though it is also sensitive to gravitational memory. It is also equivalent to computing the Newman–Penrose observable  $\Psi_4$ , all other Newman–Penrose quantities being subleading in  $1/r$ . Non-linearities in the metric are asymptotically suppressed given the enormous distance  $r$  of the observer from the source. This is by far the largest scale in our calculation. We may also note that the operator  $\mathcal{O}_\mathcal{W}$  is invariant under diffeomorphisms which vanish when  $r \rightarrow \infty$ .<sup>1</sup>

Our setup is characterized by the following hierarchy of scales,

$$\frac{1}{m_i} \ll Gm_i \ll |b| \ll r, \quad (\text{II.7})$$

<sup>1</sup> The waveform is not invariant under large diffeomorphisms, which introduce an angular-dependent phase shift [80–82]. This phase shift will be irrelevant for collaborations of terrestrial or near-Earth observatories, given the attostopic size of the angles involved.

where the first corresponds to the classical limit, and the second to the validity of relativistic perturbation theory. The expansion parameters for observables of interest are the quantities  $Gm_i/|b|$ . We take these two to be parametrically equivalent. In intermediate steps in our computations, we may see the appearance of terms which go as  $Gm_i^2$ ; these are sometimes called *classically singular terms*. Such terms will cancel in the final expression for physical observables<sup>2</sup>. At leading order in the  $1/r$  expansion, the full metric includes the backgrounds of the scattering objects in addition to the waveform we compute. Only on-shell modes contribute to the waveform. Expressing the waveform operator in terms of creation and annihilation operators, and using an asymptotic approximation we find [50] the following expression for the time-domain waveform,

$$\widetilde{\mathcal{W}}_h(u, \hat{\mathbf{n}}) = \frac{1}{4\pi r} \int_0^\infty \hat{d}\omega [e^{-i\omega u} \mathcal{W}_h(\omega, \hat{\mathbf{n}}) + \text{c.c.}], \quad (\text{II.8})$$

where  $u = t - r$  is the *retarded time* with  $t$  the time as measured by the observer and  $\mathcal{W}_h(\omega, \hat{\mathbf{n}})$  the frequency-domain waveform<sup>3</sup>:

$$\begin{aligned} \mathcal{W}_h(\omega, \hat{\mathbf{n}}) = & \\ & \kappa \int d\mu \left[ \mathcal{M}(p_1 p_2 \rightarrow p'_1 p'_2 k^{-h}) \right. \\ & \left. - i \mathcal{M}(p_1 p_2 \rightarrow X k^{-h}) \otimes_X^{(+)} \mathcal{M}^*(p'_1 p'_2 \rightarrow X) \right]; \end{aligned} \quad (\text{II.9})$$

$k^\mu = \omega n^\mu = \omega(1, \hat{\mathbf{n}})$  (with  $\hat{\mathbf{n}}$  a unit spatial vector pointing in the direction of the observer at spatial infinity); the operator  $\otimes_X^{(+)}$  denoting a sum over all intermediate states  $X$ ; and the on-shell measure is defined as,

$$\begin{aligned} d\mu = & \prod_{i=1}^2 \hat{d}^D q_i \hat{\delta}(2p_i \cdot q_i - q_i^2) e^{ib_i q_i} \hat{\delta}^D(q_1 + q_2 - k) \\ = & \hat{d}^D q \hat{\delta}(2\bar{p}_1 \cdot q) \hat{\delta}(2\bar{p}_2 \cdot (k - q)) e^{ik \cdot b_2 + ib \cdot q}, \end{aligned} \quad (\text{II.10})$$

where  $q_i^\mu = p_i^\mu - p_i'^\mu$  is the *mismatch* between the incoming and outgoing wavepackets; in the second line of Eq. (II.10), we have introduced shifted momenta,

$$\bar{p}_i^\mu = p_i^\mu + \frac{q_i^\mu}{2}. \quad (\text{II.11})$$

The complex conjugation in Eq. (II.8) is needed to ensure that the waveform in the *time domain* is real, once

<sup>2</sup> If we perform our computations using the Schwinger–Keldysh formalism instead of the scattering-amplitudes approach, classically singular terms do not appear even at intermediate steps. This simplification comes at the cost of computing integrals with retarded and advanced propagators rather than Feynman, or anti-Feynman ones.

<sup>3</sup> Here, we combined a factor of  $-i$  from the definition of the waveform with an  $i$  from rewriting the  $S$ -matrix operator in terms of the transfer matrix. Note that  $\mathcal{W}_h(\omega, \hat{\mathbf{n}})$  has dimension [energy]<sup>-2</sup> in four dimensions.

we strip off the polarization tensor  $\varepsilon_{\mu\nu}$ . We write the polarization tensor in double-copy form, as a product of spin-1 polarization vectors,

$$\varepsilon_{\mu\nu}^{(h)} = \varepsilon_\mu^{(h/2)} \varepsilon_\nu^{(h/2)}. \quad (\text{II.12})$$

The first term in the second line of Eq. (II.9) represents an in–out observable, *i.e.* a  $2 \rightarrow 3$  scattering amplitude. The second term is needed to subtract classically-singular contributions and to restore the correct causality properties. The latter are dictated by retarded propagators, ensuring that overall we obtain an in–in observable [54]. We emphasize that Eq. (II.8) is valid strictly in four dimensions, whereas the frequency domain expression (II.9) is valid in generic dimension  $D$ .

In the following calculations, we will perform both the loop and Fourier integrals in  $D = 4 - 2\epsilon$ . We then take the limit  $\epsilon \rightarrow 0$ . We treat Fourier and loop momenta on the same footing, allowing us to express frequency-space waveforms in terms of a minimal basis of functions which we denote *combined master integrals* (CMIs):

$$\mathcal{W}_h(\omega, \hat{\mathbf{n}}) = \sum_{i=1}^n c_i I_i. \quad (\text{II.13})$$

Here,  $n$  is the number of combined master integrals. It turns out that the basis described here is not limited to scalar scattering but also suffices to express waveforms for spinning objects.

*Kinematics* Expressions for the five-point process depend on the incoming and outgoing momenta of the two massive particles, the emitted graviton momentum, and the impact parameter. We can parametrize the massive momenta as

$$p_i^\mu = m_i u_i^\mu, \quad (\text{II.14})$$

where the  $u_i^\mu$  are the classical four-velocities of the two particles. As emphasized above in the definition of the Fourier measure (II.10), it is convenient to consider the classical limit of the in–in observable around shifted momenta  $\bar{p}_i^\mu$ , which we can parametrize analogously to Eq. (II.14),

$$\bar{p}_i^\mu = \bar{m}_i \bar{u}_i^\mu = m_i u_i^\mu + \frac{q_i^\mu}{2}. \quad (\text{II.15})$$

In following sections, we shall work with barred variables. After computing the Fourier transform, the difference between  $u_i^\mu$  and  $\bar{u}_i^\mu$  will amount to a correction of order  $\frac{1}{m|b|}$ , which is negligible according to the hierarchy (II.7). We will keep the barred variables throughout the computation for clarity, and drop the bar in the final result.

The frequency-domain waveform depends on five independent Lorentz invariants constructed from the four-vectors  $\{u_1^\mu, u_2^\mu, b^\mu, k^\mu\}$ ,

$$\gamma = u_1 \cdot u_2, \quad w_1 = u_1 \cdot k, \quad w_2 = u_2 \cdot k, \quad b^2, \quad b \cdot k. \quad (\text{II.16})$$

The vectors also satisfy the following relations:

$$u_i^2 = 1, \quad u_i \cdot b = 0, \quad k^2 = 0. \quad (\text{II.17})$$

We also define a norm,

$$\mathbf{b} = \sqrt{-b^2}. \quad (\text{II.18})$$

### III. COMPUTATIONAL STEPS

The computation of the analytic one-loop gravitational waveform proceeds in several steps, previously presented [1] by two of the authors,

1. *Integrand computation.* We select only contributions that can yield terms non-analytic in the  $q_i^2$ . The Fourier transform from  $q$ -space to impact-parameter space will turn analytic terms into local interactions, which will not contribute to the observable. Such terms may be extracted using generalized unitarity cuts [56] in the corresponding channels, as shown in Fig. (1). This corresponds to *sewing* lower-loop and lower-point amplitudes. The latter amplitudes are obtained by first taking the heavy-mass expansion [26, 62] on both sides of each cut. This is suggested by the classical limit in Eq. (II.7) [83], which significantly reduces the maximum rank of the tensors in the power counting.
2. *Mapping in-out to in-in.* As mentioned in the previous section, both terms inside the brackets in Eq. (II.9) contain terms singular in the classical limit. These cancel in the final result, after the terms are combined. On the other hand, we know that the Feynman rules of the two terms are identical up to  $i\epsilon$ s. Therefore, in principle, it is sufficient to understand how propagators combine when we sum over appropriate  $i\epsilon$  coefficients in a simplified context, *e.g.* a scalar theory, and assign the corresponding prescriptions to the integrand previously determined. This strategy has been used in Ref. [54] to show for the one-loop classical waveform that the map from the in-out formulation to the in-in one for an observable corresponds to substituting *retarded propagators* for Feynman propagators (which in the classical limit would have become principal-valued linearized propagators).
3. *Tensor and IBP reduction.* In order to avoid the appearance of unphysical poles in intermediate steps, we treat Fourier and loop momenta on the same footing. For example, tensor decompositions can be performed as though the integrand was that of a two-loop integral; the exponential factor does not play a role. In contrast, IBP relations are modified, and we will find fewer of them than for a pure two-loop integral. As we shall see, IBP relations for combined Fourier-loop integrals are linear combinations of IBP relations for the loop integrals.
4. *Loop and Fourier integrals.* Once the waveform is expressed in terms of a basis of CMIs, we must evaluate them. We do this loop by loop, first computing

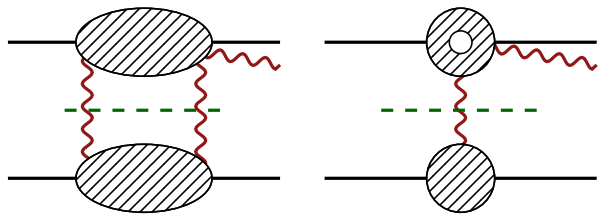


FIG. 1. Generalized unitarity cuts probing the singularities at  $q_i^2 = 0$  at one-loop. Left: double graviton exchange. Right: single graviton exchange with the one-loop gravitational Compton amplitude on one side of the cut. This figure has been copied from Ref. [1].

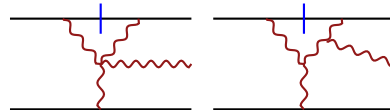


FIG. 2. When considering one-particle and two-particle generalized unitarity cut in general relativity, there are overlapping contributions due to the nonlinear nature of General Relativity. These diagrams give non-zero contributions in taking residues and discontinuities at  $q_i^2 = 0$ .

the one-loop integrals, and then their Fourier transforms. At higher order, it will be worth exploring using differential equations directly on the CMIs.

Let us now discuss some of the technical details of the steps above.

*a. Integrand and Generalized Unitarity.* We can construct the integrand for combined Fourier and loop integrand using generalized unitarity. The quantum amplitude has several (generalized) unitarity cuts, involving the massive states and/or the gravitons. In the classical limit, singularities corresponding to cuts of massive lines are pushed to infinity in the  $q_i^2$ . The relevant cuts for the Fourier transform are then only those associated to on-shell massless particles, shown in Fig. 1.

At one loop the building blocks needed to construct the integrand are the tree-level amplitudes with up to three gravitons and the one-loop gravitational Compton amplitude. The former have been computed in Ref. [62] within the heavy-mass expansion. This expansion offers a power-counting in the masses, allowing us to distinguish genuine higher-order corrections from classically singular terms (see also Refs. [22, 84] for equivalent tree-level amplitudes). The sewing of the Compton amplitude is performed prior to the loop integration, in order to avoid multiple counting of contributions probed both by the one-particle and the two-particle cuts (*e.g.* as in Fig. 2). We can obtain a gauge-invariant form of the Compton integrand by combining generalized unitarity cuts in two different channels using a permutation-symmetric ansatz. We give more details on integrand construction for the Compton and the five-point integrands in Appendices B and C. Both our integrands are

linear in the linearized Riemann tensor of the external gravitons,

$$R_{\mu\nu\rho\sigma} = k_\mu k_\nu \varepsilon_{\rho\sigma} - k_\nu k_\rho \varepsilon_{\mu\sigma} - k_\mu k_\sigma \varepsilon_{\nu\rho} + k_\rho k_\sigma \varepsilon_{\mu\nu} . \quad (\text{III.1})$$

This ensures gauge invariance at each step of the computation. For the internal graviton state sums we use,

$$\sum_h \varepsilon_{\mu\nu}^{(h)}(k) \varepsilon_{\rho\sigma}^{(-h)}(-k) = \frac{P_{\mu\rho} P_{\nu\sigma} + P_{\mu\sigma} P_{\nu\rho}}{2} - \frac{P_{\mu\nu} P_{\rho\sigma}}{D_s - 2} , \quad (\text{III.2})$$

where,

$$P_{\mu\nu} = \eta_{\mu\nu} - \frac{k_\mu r_\nu + k_\nu r_\mu}{k \cdot r} + r^2 \frac{k_\mu k_\nu}{(k \cdot r)^2} , \quad (\text{III.3})$$

in which  $r_\mu$  is a reference vector in axial quantization and  $D_s - 2$  is the number of spin degrees of freedom of the graviton in dimensional regularization. We consider two distinct regularization schemes: the ‘t Hooft-Veltman (HV) scheme<sup>4</sup> with  $D_s = D = 4 - 2\epsilon$  and the four-dimensional helicity (FDH) [85] or dimensional-reduction (DR) schemes with  $D_s = 4$  [86]. The latter two are equivalent at one loop.

The integrand is provided in the ancillary file `integrand.m`. We expect the tensor reduction of the integrand constructed as above to yield results equivalent to those obtained in Refs. [51, 52, 55]. Indeed, we find that the difference between our results and those of the latter references is polynomial in both  $q_1^2$  and  $q_2^2$  (for example, see the re-organization of the waveform in terms of transcendental functions free of spurious poles in Ref. [82]). Such terms would give local contributions in impact-parameter space. We are able to remove all such terms, which are of no interest to observers located very far from the source. The integrand computation can be performed entirely within the heavy-mass approximation, without needing the subtle contributions from the so-called *snail* diagrams; such terms were computed in Refs. [51, 52] through subtle forward limits as some of the relevant contributions could not be captured through two-particle cuts over internal graviton legs. In our approach, these contributions are captured by the single-graviton cuts shown in the right-hand diagram in Fig. 1.

*b. Integrand reduction.* The frequency-space one-loop contributions to the NLO waveform are analogous to a two-loop integral,

$$\mathcal{W}_h^{(1)}(\omega, \hat{\mathbf{n}}) = \frac{e^{i\omega \hat{\mathbf{n}} \cdot \mathbf{b}_2}}{4\pi r} \int_{\hat{q}, \hat{\ell}} e^{ib \cdot q} T^{(1)} , \quad (\text{III.4})$$

where we treat the Fourier transform to impact-parameter space on an equal footing with the loop-momentum integration. The integrand appearing in Eq. (III.4) contains tensor structures in which the linearized Riemann tensor is contracted either with the loop or the Fourier momentum. We perform the tensor reduction following Ref. [87] where the four-dimensional space of external momenta is spanned by the vectors  $u_1^\mu$ ,  $u_2^\mu$ ,  $b^\mu$  and  $k^\mu$ . We need to reduce tensors with up to four powers of an integrated momentum. Whenever one of these momenta is contracted with an external momentum (rather than with the Riemann tensor), the projectors defined in Ref. [87] simply reproduce the given momentum. We provide the explicit form of the required projectors in Appendix D.

After tensor reduction, we obtain a sum of integrals with nontrivial numerators but no free indices. Each integral belongs generalized integral family,

$$I_{a_1 \dots a_{11}}[\mathcal{N}(q, \ell)] = \int_{\hat{q}, \hat{\ell}} \frac{e^{D_1} \mathcal{N}(q, \ell)}{\prod_{i=1}^{11} D_i^{a_i}} , \quad (\text{III.5})$$

where the invariants  $D_i$  are,

$$\begin{aligned} D_1 &= iq \cdot b, & D_2 &= q^2, & D_3 &= (q - k)^2, \\ D_4 &= \bar{u}_1 \cdot q, & D_5 &= \bar{u}_2 \cdot (k - q), & D_6 &= \bar{u}_1 \cdot \ell, \\ D_7 &= \bar{u}_2 \cdot \ell, & D_8 &= \ell^2, & D_9 &= (\ell + q)^2, \\ D_{10} &= (\ell + q - k)^2, & D_{11} &= ib \cdot \ell. \end{aligned} \quad (\text{III.6})$$

Of these invariants,  $D_{1,11}$  can appear only as numerators;  $D_{4,5}$  appear as delta functions because of the LIPS measure; and either  $D_6$  or  $D_7$  are localized on-shell by the classical limit. We can therefore restrict attention to two subfamilies, the first:

$$I_{a_1, a_2, a_3, 1, 1, 1, a_7, \dots, a_{11}}^{(1)}[\mathcal{N}(q, \ell)] = \int_{\hat{q}, \hat{\ell}} e^{D_1} \hat{\delta}(D_4) \hat{\delta}(D_5) \hat{\delta}(D_6) \frac{D_1^{-a_1} D_{11}^{-a_{11}}}{D_2^{a_2} D_3^{a_3} D_7^{a_7} D_8^{a_8} D_9^{a_9} D_{10}^{a_{10}}} , \quad (\text{III.7})$$

<sup>4</sup> Recall that the HV scheme keeps external momenta four-dimensional, while the conventional scheme keeps them  $D$ -dimensional. Restricting the external kinematics to four dimensions simplifies tensor reductions.

with the second  $I^{(2)}$  obtained from  $I^{(1)}$  by exchanging  $D_6 \leftrightarrow D_7$ . These are *twisted period integrals* [74]. It is possible to decompose them into a finite basis of independent integrals, the so-called *master integrals*, either via intersection theory [74, 88, 89] or via generalized IBP

identities [1]:

$$\int_{\hat{q}, \hat{\ell}} \frac{\partial}{\partial r^\mu} \left( \frac{e^{D_1} v^\mu}{\prod_{i=1}^{11} D_i^{a_i}} \right) = 0, \quad r^\mu \in \{\ell^\mu, q^\mu\} \quad (\text{III.8})$$

$$\text{IBP}_{a_1, \dots, a_{11}}[\mathcal{N}(q, \ell)] = \int_{\hat{q}, \hat{\ell}} \mathcal{N}(q, \ell) \frac{\partial}{\partial r^\mu} \left( \frac{v^\mu}{\prod_{i=1}^{11} D_i^{a_i}} \right), \quad r^\mu \in \{\ell^\mu, q^\mu\} \quad (\text{III.9})$$

via,<sup>5</sup>

$$\text{IBP}_{a_1, \dots, a_{11}}[1 - D_1] + \text{IBP}_{a_1-1, \dots, a_{11}}[1] = 0, \quad (\text{III.10})$$

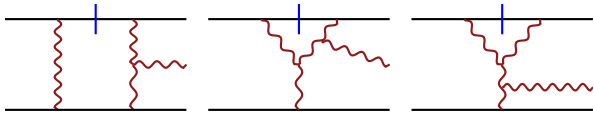


FIG. 3. Integrals arising from the application of IBP identities to the one-loop amplitude for combined Fourier and loop integrals can be reorganized into one of these three topologies, ordered as in Eq. (III.11). The integral family of Eq. (III.7) includes additional master integrals, but they do not contribute to the final result.

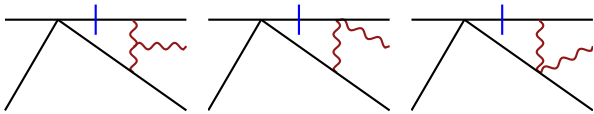


FIG. 4. One-loop diagrams with a pinched graviton propagator  $D_8$  arise when applying IBPs solely to the loop integration, but vanish in the final result after both Fourier and loop IBP reduction.

$$\begin{aligned} I_{a_1 a_2 a_3 111 a_7 \dots a_{11}}^{(1)} &= \int_{\hat{q}, \hat{\ell}} \hat{\delta}(D_4) \hat{\delta}(D_5) \hat{\delta}(D_6) \frac{e^{D_1} D_1^{-a_1} D_2^{-a_2} D_3^{-a_3} D_{11}^{-a_{11}}}{(D_7 + i\epsilon)^{a_7} D_8^{a_8} D_9^{a_9} D_{10}^{a_{10}}}, \\ I_{a_1 a_2 a_3 111 a_7 \dots a_{11}}^{(1)} &= \int_{\hat{q}, \hat{\ell}} \hat{\delta}(D_4) \hat{\delta}(D_5) \hat{\delta}(D_6) \frac{e^{D_1} D_1^{-a_1} D_2^{-a_2} D_7^{-a_7} D_{11}^{-a_{11}}}{D_3^{a_3} D_8^{a_8} D_9^{a_9} D_{10}^{a_{10}}}, \\ I_{a_1 a_2 a_3 111 a_7 \dots a_{11}}^{(1)} &= \int_{\hat{q}, \hat{\ell}} \hat{\delta}(D_4) \hat{\delta}(D_5) \hat{\delta}(D_6) \frac{e^{D_1} D_1^{-a_1} D_7^{-a_7} D_{10}^{-a_{10}} D_{11}^{-a_{11}}}{D_2^{a_2} D_3^{a_3} D_8^{a_8} D_9^{a_9}}. \end{aligned} \quad (\text{III.11})$$

We emphasize that triangle and box loop integrals

<sup>5</sup> Should we consider total derivatives with respect to the loop momentum, the second and third terms in Eq. (III.10) cancel and we recover standard IBP relations, as expected. In Eq. (III.10),  $v^\mu$  must be the same for all terms.

Localized propagators ( $D_{4,5}$  and either  $D_6$  or  $D_7$ ) can be treated as denominators via reverse unitarity [90–92]. The IBP relations for the combined Fourier and loop integrals can be written in terms of the IBP relations of ordinary integrals (without exponentials),

The generalized IBP relations can be generated systematically using one of the standard IBP codes; we have used LiteRed [67]. We solve the generalized IBP system using LiteRed and finite-field techniques as implemented in FiniteFlow [69] (which follows the Laporta algorithm [65]). Each of the two integral subfamilies  $I^{(1,2)}$  can be decomposed in terms of 76 combined master integrals. Only 28 of these integrals actually appear in the result for the waveform. This simplification can be understood in terms of the Feynman diagrams contributing to the process. All terms in the integrand are daughters of the following three topologies (see Fig. 3),

with pinched  $D_8$  (see Fig. 4) never appear in the combined Fourier and loop approach, whereas they would were we to follow a loop-only reduction, as was done in Refs. [51, 52, 55]. Indeed, in such an approach, although their final contributions would be polynomial in  $q_1^2$  and  $q_2^2$  (and hence local and of no interest), they would appear multiplied by rational functions of the  $q_i^2$ . One would

therefore expect them to contribute nontrivially to the waveform. We choose the CMIs so that their rational coefficients are finite as  $\epsilon \rightarrow 0$ , using the algorithm presented in Ref. [93]. We split them into two sets: 16 ‘base’ integrals and 12 ‘derivative’ integrals (indicated below by underlining) which can be obtained from the former by taking a derivative with respect to the impact parameter  $b$ . In particular, we have

$$\begin{aligned}
& \bullet I_{00111100110}^{(1)} ; \quad \underline{I_{-10111100110}^{(1)}} \\
& \bullet I_{00011101100}^{(1)} , \quad I_{00111101100}^{(1)} , \quad I_{0-1111101100}^{(1)} , \\
& \quad \underline{I_{00211101100}^{(1)}} ; \quad \underline{I_{-10011101100}^{(1)}} , \quad \underline{I_{-10111101100}^{(1)}} \\
& \bullet I_{00011101010}^{(1)} , \quad I_{00111101010}^{(1)} ; \quad \underline{I_{-10011101010}^{(1)}} , \\
& \quad \underline{I_{-10111101010}^{(1)}} \\
& \bullet I_{00011101110}^{(1)} , \quad I_{001111-11110}^{(1)} , \quad I_{0011110111-1}^{(1)} , \\
& \quad I_{00111101110}^{(1)} , \quad I_{0-1111101110}^{(1)} , \quad I_{00111102110}^{(1)} ; \\
& \quad \underline{I_{-10011101110}^{(1)}} , \quad \underline{I_{-101111-11110}^{(1)}} , \quad \underline{I_{-1011110111-1}^{(1)}} , \\
& \quad \underline{I_{-10111101110}^{(1)}} \\
& \bullet I_{00011111100}^{(1)} , \quad I_{00011111010}^{(1)} , \quad I_{00011111110}^{(1)} ; \\
& \quad \underline{I_{-10011111100}^{(1)}} , \quad \underline{I_{-10011111010}^{(1)}} , \quad \underline{I_{-10011111110}^{(1)}} .
\end{aligned}$$

Each bullet corresponds to a different topology in the combined momenta. The result in terms of combined MIs multiplied by their rational coefficients is provided in the ancillary file `reduced_integrand.m`.

*c. Integration.* We have yet to explore a systematic approach to the combined integrals using differential equations. Instead, we have performed the integrations sequentially. We first evaluated the loop integrals using canonical differential equations, following Ref. [1]. We computed the Fourier transform afterwards. We record the required loop integrals in Appendix E. We find it helpful to split the second integration into two pieces, performing the Fourier transforms of the infrared-divergent and -finite terms separately. The Fourier transform does not introduce additional divergences; we must however treat  $\epsilon/\epsilon$  terms carefully, as they are physically relevant at one-loop [82]. Accordingly, we need a proper  $D$ -dimensional measure for the Fourier integrals to compute them correctly. In contrast, the Fourier transform of the finite part can be performed using the four-dimensional measure as introduced in Ref. [50]. We provide details of the integration in Appendix F. The integrals are available upon request from the authors.

#### IV. COMPARISONS WITH PREVIOUS RESULTS

We can separate terms in the one-loop contributions to the waveform into infrared-divergent ones, the corre-

sponding logarithms, so-called *tail terms* [94], and finite ones,

$$\mathcal{W}_h^{(1)} = \mathcal{W}_{h,\text{IR}}^{(1)} + \mathcal{W}_{h,\text{tail}}^{(1)} + \mathcal{W}_{h,\text{fin}}^{(1)} , \quad (\text{IV.1})$$

where,

- $\mathcal{W}_{h,\text{IR}}^{(1)}$  is the infrared-divergent part. It is proportional to the tree-level frequency-domain waveform [54, 95] (presented in Appendix A):

$$\mathcal{W}_{h,\text{IR}}^{(1)} = i \frac{\kappa^2 s_W}{\epsilon} \mathcal{W}_h^{(0)} , \quad (\text{IV.2})$$

where the prefactor  $s_W$  is

$$s_W = \frac{m_1 w_1 + m_2 w_2}{32\pi} \Gamma_\alpha , \quad (\text{IV.3})$$

in which,

$$\Gamma_\alpha = 1 - \alpha \frac{\gamma(\gamma^2 - \frac{3}{2})}{(\gamma^2 - 1)^{3/2}} , \quad (\text{IV.4})$$

with  $\alpha = -1, 0$  as in Appendix E. The values of  $\alpha$  correspond to two different choices of classical boundary conditions:

- $\alpha = -1$  corresponds to an *asymmetric* choice of frame between incoming and outgoing momenta. Here,  $p_{i,\text{in}}^\mu = p_i^\mu$  and  $p_{i,\text{out}}^\mu = p_i^\mu - \Delta p_i^\mu$ , where  $\Delta p_i^\mu$  is the impulse on the  $i^{\text{th}}$  particle. This is the frame typically used in the KMOC formalism [49, 50].
- $\alpha = 0$  corresponds to the *symmetric* frame for which  $p_{i,\text{in}}^\mu = p_i^\mu + \Delta p_i^\mu/2$  and  $p_{i,\text{out}}^\mu = p_i^\mu - \Delta p_i^\mu/2$ . This is the frame usually chosen in so-called ‘multipolar post-Minkowskian’ computations, where classical boundary conditions are fixed at  $t = 0$ , rather than at  $t = -\infty$  [96]. At NLO, this frame is related to the previous one through dropping the contribution of the cut terms in the KMOC formalism in the classical limit. Their contribution is then equivalent to performing the corresponding rotation [81].

The infrared divergences exponentiate to an overall phase in the waveform in frequency space [54, 95],

$$\mathcal{W}_h(\omega, \hat{\mathbf{n}}) = e^{-i\kappa^2 s_W/\epsilon} \mathcal{W}_{h,\text{DR}}(\omega, \hat{\mathbf{n}}), \quad (\text{IV.5})$$

where DR in the subscript stands for dimensional regularisation. Inside the right-hand side, we keep terms of higher order in  $\epsilon$ . The infrared-divergent phase encodes information about different time delays due to the long-range nature of the gravitational interactions in four dimensions (for a clear discussion of the physical interpretation of this divergences, we refer to Ref. [54]). On the other hand, an overall phase is not relevant to gravitational-wave observations. Indeed, in the time domain, it corresponds to a constant shift of the arrival time of the gravitational wave. This is *a priori* non measurable. When extracting a signal from the background noise, a filter is applied with different time shifts to search for the signal at an *a priori* undetermined time (see the discussion in Ref. [97]).

- $\mathcal{W}_{h,\text{tail}}^{(1)}$  contains the ‘tail’ terms. These express the effect of rescattering of the emitted gravitational waves by the background generated by the two-body system at large distances. This includes a modification of the group velocity [98]. Given our standard use of infinite interaction time<sup>6</sup>, these effects manifest themselves in an infrared divergence. The infrared divergence exponentiates and it is accompanied by a finite logarithm (which also exponentiates). At fixed order we have logarithms; at NLO we have a single logarithm proportional to the lowest-order waveform:

$$\mathcal{W}_{h,\text{tail}}^{(1)} = i\kappa^2 s_W \log\left(\frac{\omega^2}{4\pi\mu^2}\right) \mathcal{W}_h^{(0)}, \quad (\text{IV.6})$$

where  $\mu^2$  is an (infrared) scale. The precise definition of this scale does not affect observables, as different choices of  $\mu^2$  correspond to changes in the phase of the waveform, *i.e.* to a finite redefinition of the observer’s clock reference time.

- $\mathcal{W}_{h,\text{fin}}^{(1)}$  are new contributions which are not proportional to the lowest-order ones. We focus mainly on these terms in frequency-domain plots below. In Eq. (IV.5),  $\mathcal{W}_{h,\text{DR}}$  is computed to all orders in  $\epsilon$ . When we expand Eq. (IV.5), we will pick up finite contributions which arise from the cancellations of the singular expansion of the phase against  $\epsilon$ ’s in  $\mathcal{W}_{h,\text{DR}}$ . These terms should be excluded from the observable waveform. We can expand the  $\mathcal{W}_{h,\text{DR}}$  in  $\epsilon$ ,

$$\mathcal{W}_{h,\text{DR}} = \mathcal{W}_{h,\text{obs}} + \epsilon \mathcal{W}_{h,\epsilon} + \mathcal{O}(\epsilon^2), \quad (\text{IV.7})$$

where  $\mathcal{W}_{h,\text{obs}}$  is free of  $\epsilon$ -dependence. The  $\epsilon/\epsilon$  term should be excluded from the observable waveform, which is then,

$$\mathcal{W}_{h,\text{obs}}^{(1)} = \mathcal{W}_{h,\text{fin}}^{(1)} - i\kappa^2 s_W \mathcal{W}_{h,\epsilon}. \quad (\text{IV.8})$$

## A. Comparison with other calculations

Several groups have computed the fully relativistic scalar NLO waveform in momentum space using amplitudes techniques [51–53]. Two of these groups [51, 52] also used the KMOC formalism. In addition, Ref. [55, 99] also computed the NLO waveform for spinning particles, using the WQFT formalism [78]. The results in Refs. [51–53] were previously compared and found to agree. We have compared our results with those of Ref. [51], after loop integration, but before the FT. We find complete agreement up to local terms (such as polynomial terms in  $q_1^2$  and  $q_2^2$ ), which are irrelevant in the classical limit. We would not expect local terms to agree, because our construction of the integrand drops them.

## B. The center-of-momentum frame

We can generate frequency-domain plots for the finite part  $\mathcal{W}_{h,\text{fin}}^{(1)}$ . We choose the symmetric frame discussed above for our numerical evaluation. Define four orthonormal vectors: a time-like  $e_0^\mu$ , and three space-like  $e_i^\mu$  ( $i = 1, 2, 3$ ). The (adjusted) momenta of the two bodies are,

$$p_1^\mu = E_1 e_0^\mu + P_{\text{cm}} e_2^\mu, \quad p_2^\mu = E_2 e_0^\mu - P_{\text{cm}} e_2^\mu, \quad (\text{IV.9})$$

with  $E_i = \sqrt{m_i^2 + P_{\text{cm}}^2}$ , and  $P_{\text{cm}}$  the momentum in the symmetric frame. We can rewrite these quantities in terms of the masses and the Lorentz boost introduced earlier,

$$P_{\text{cm}} = \frac{m_1 m_2 \sqrt{\gamma^2 - 1}}{E}, \quad E = E_1 + E_2 = \sqrt{m_1^2 + m_2^2 + 2m_1 m_2 \gamma}. \quad (\text{IV.10})$$

We choose the impact parameters  $b_1$  and  $b_2$  to be,

$$b_1^\mu = \frac{E_2}{E} b^\mu, \quad b_2^\mu = -\frac{E_1}{E} b^\mu, \quad b^\mu = \mathbf{b} e_1^\mu. \quad (\text{IV.11})$$

Because the observer is very far away from the scattering, the momentum  $k^\mu$  of the emitted graviton is essentially fixed to be along the direction towards the observer. Thus, its momentum and polarization tensor  $\varepsilon^{\mu\nu} = \varepsilon^\mu \varepsilon^\nu$  are given in terms of,

$$k^\mu = \omega [e_0^\mu + n^\mu(\theta, \phi)], \quad \varepsilon_{(\pm)}^\mu = \frac{1}{\sqrt{2}} \left( \partial_\theta n^\mu(\theta, \phi) \mp \frac{i}{\sin\theta} \partial_\phi n^\mu(\theta, \phi) \right), \quad (\text{IV.12})$$

<sup>6</sup> That is ignoring frequency band limits and noise floor limits of any realistic detectors.

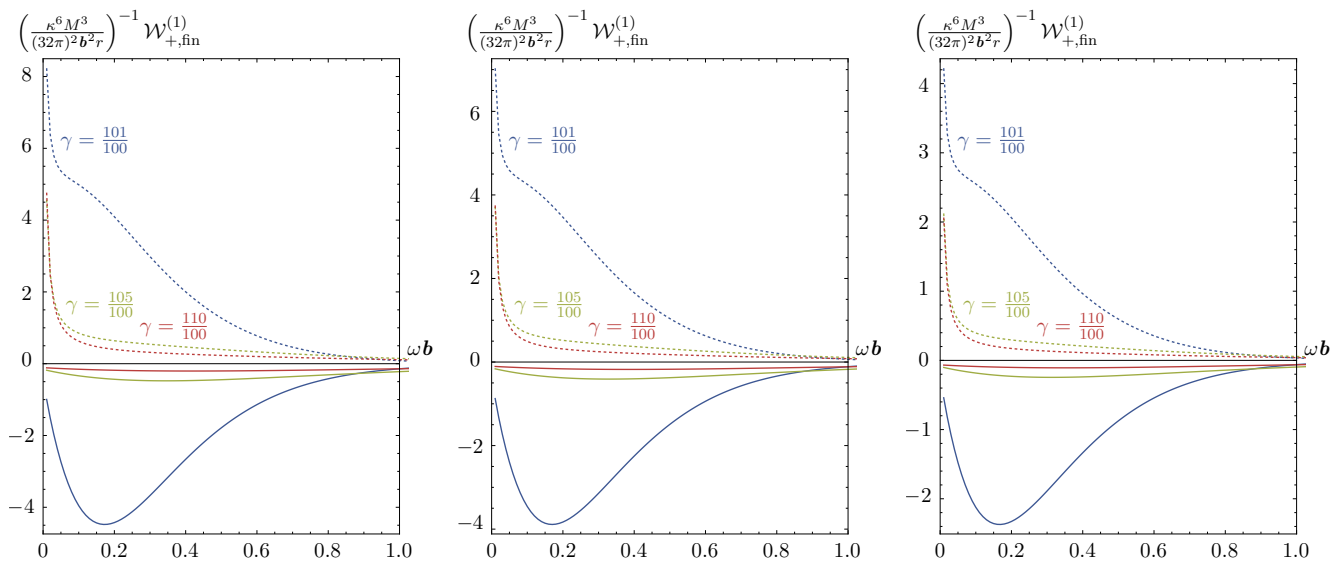


FIG. 5. Plots of the finite part of the NLO frequency-domain waveform  $\mathcal{W}_{h,\text{fin}}^{(1)}$ , for the  $[+]$  polarization. Each plot show different values of the boost  $\gamma$  with fixed symmetric mass ratio  $\nu$ , which are, respectively  $\{\frac{1}{4}, \frac{2}{9}, \frac{5}{36}\}$ . The plots are at the fixed angle  $(\theta, \phi) = (\frac{7\pi}{5}, \frac{7\pi}{10})$ . Solid lines represent the real part, while dashed lines represent the imaginary part.

where  $n^\mu(\theta, \phi)$  is the unit space-like vector pointing in the direction of the observation:

$$n^\mu(\theta, \phi) = \sin\theta \cos\phi e_1^\mu + \sin\theta \sin\phi e_2^\mu + \cos\theta e_3^\mu. \quad (\text{IV.13})$$

In our case, we are interested in computing the waveforms for the  $[+]$ ,  $[\times]$  polarizations of the graviton; these are defined in terms of the helicities as follows,

$$\begin{aligned} \varepsilon_{[+]}^{\mu\nu} &= \frac{1}{2} \left( \varepsilon_{(-)}^\mu \varepsilon_{(-)}^\nu + \varepsilon_{(+)}^\mu \varepsilon_{(+)}^\nu \right), \\ \varepsilon_{[\times]}^{\mu\nu} &= \frac{1}{2i} \left( \varepsilon_{(-)}^\mu \varepsilon_{(-)}^\nu - \varepsilon_{(+)}^\mu \varepsilon_{(+)}^\nu \right), \end{aligned} \quad (\text{IV.14})$$

We can write our result in terms of the total mass of the system  $M$  and the symmetric mass ratio  $\nu$ ,

$$M = (m_1 + m_2), \quad \nu = \frac{m_1 m_2}{(m_1 + m_2)^2}; \quad (\text{IV.15})$$

we use the latter as one of the parameters in the plots.

### C. Visualization of results

In Fig. 5 we show the NLO corrections to the frequency domain waveform at fixed angle  $(\theta = \frac{7\pi}{10}, \phi = \frac{7\pi}{5})$  for different values of the symmetric mass ratio  $\nu$  and of the Lorentz factor  $\gamma$ . One of the interesting aspects of our approach is the simplification of the Fourier transform to impact-parameter space, as it is now written as a one-dimensional integral over an exponentially-damped integrand involving at worst logarithms and square roots. This allows for fast numerical evaluation, avoiding spurious singularities on the integration contour. Indeed, the

combined Fourier and loop IBP relations trade the would-be spurious poles in  $q_i^2$  for Gram determinants outside the integration. There is only a small price to pay: close to certain kinematic points, the numerical integration requires higher precision, as cancellations occur between different MIs and their rational coefficients. For example, at  $\theta = 0, \pi$  we have spurious poles corresponding to kinematic configurations where  $b \cdot k = 0$ .

### D. Post-Newtonian Expansion

In order to compare our result with the GR results of Ref. [82, 96], we can expand our result in terms of the dimensionless velocity parameter  $p_\infty$  after changing variables,

$$\gamma = \sqrt{1 + p_\infty^2}, \quad \omega = p_\infty \Omega_\infty, \quad (\text{IV.16})$$

with  $\Omega_\infty$  the frequency of the emitted graviton. In this work, we have kept so far the state-counting dimensional regularization parameter  $D_s$  arbitrary. In the following, we will set  $D_s = 4$  for the graviton state counting, *i.e.* we will work within the so-called FDH or DR schemes, which are equivalent at one loop. This includes performing the FT in  $D = 4 - 2\epsilon$  dimensions. Would we have chosen instead  $D_s = D$ , additional  $\epsilon/\epsilon$  contributions would appear. These arise from the  $\epsilon$ -expansion of both the finite and infrared-divergent parts of the amplitude. Such terms would ultimately cancel when including corrections higher order in  $\epsilon$  to the tree-level waveform.

To perform the comparison, we work with  $\alpha = 0$ , and in the center-of-momentum frame. We expand our result using Eq. (IV.16). We choose numerical values for

the angles, the impact parameter, the frequency and the masses. We choose integer values for the frequency, the impact parameter and the masses. Two particular combinations of the polar angles appear,

$$z = e^{i\phi} \cot \theta, \quad \bar{z} = e^{-i\phi} \cot \theta. \quad (\text{IV.17})$$

We choose integer values for  $z$  and  $\bar{z}$  as well. This ensures that all arguments of logarithms and Bessel functions are integral, and all coefficients are rational. This in turn gives us confidence that cancellations are treated exactly, without needing to worry about precision loss in the numerical evaluation. Indeed, while the NLO waveform starts at order  $1/p_\infty^3$ , in intermediate stages we find terms of order  $1/p_\infty^{41}$  (or possibly even higher). All the unwanted higher powers cancel exactly, and we are left to compare terms of order  $1/p_\infty^3$  through  $p_\infty^1$  with the GR result. The results provided in Ref. [82], are separated into terms symmetric in  $m_1 \leftrightarrow m_2$ , and those antisymmetric in the exchange. The complete set of the first were given (from  $1/p_\infty^3$  to  $p_\infty^2$ ). In the latter set, the  $1/p_\infty^3$  and  $1/p_\infty$  terms vanish, and only the  $1/p_\infty^2$  and  $p_\infty^1$  terms were given. We have compared the combined terms through order  $p_\infty^1$ , with the  $p_\infty^0$  order excluded. In particular, we have chosen<sup>7</sup>

$$b\omega = 3, \quad \frac{m_2 - m_1}{m_1 + m_2} = \frac{1}{6}, \quad z = 3 + 5i, \quad (\text{IV.18})$$

finding perfect agreement with all the terms given in Ref. [82]. We compared the observable waveform  $\mathcal{W}_{h,\text{obs}}^{(1)}$  of Eq. (IV.8) with the GR result. The latter is not computed in dimensional regularization, and accordingly has no  $\epsilon$  dependence. However, it has a dependence on the frame-dependent scale  $b_0$  [82]. We have translated the  $\epsilon$  dependence to a dependence on  $\mu$  in a standard fashion. We must now relate the scale  $\mu$  to  $1/b_0$ . The check up to order  $p_\infty^1$  does not include subtleties related to the angular-dependent redefinition of the retarded time, interpreted as the supertranslation identified by Veneziano and Vilkovisky [80] in Refs. [81, 82, 100]. The first term affected by this mapping is at order  $p_\infty^2$ . Analytic comparison at higher orders in  $p_\infty$  expansion with MPM result would be an interesting direction to pursue, for example implementing strategies recently explored in Ref. [101].

## V. THE POWER SPECTRUM

The differential power spectrum (or energy spectrum) carried by gravitational waves gives the total energy emitted per unit frequency during the scattering process. Starting from the frequency-domain waveform

$\mathcal{W}_h(\omega, \theta, \varphi)$ , it can be defined as follows,

$$\frac{dE}{d\omega} = \frac{2}{\kappa^2} \int d\Omega \sum_h |\omega \mathcal{W}_h(\omega, \Omega)|^2, \quad (\text{V.1})$$

where the solid-angle integral covers the entire celestial sphere and the sum runs over the two graviton helicities. This observable is gauge-invariant and infrared-finite and provides a clean connection between theoretical predictions and measurable quantities. The spectrum enters directly in the computation of the gravitational-wave flux and, ultimately, in the signal-to-noise ratio used by matched-filtering analysis pipelines. It has been presented analytically to high order in the PN expansion based on the expansion of the leading-order relativistic waveform [43, 102]. Here we are interested in the numerical computation of the NLO ( $\mathcal{O}(G^4)$ ) power spectrum. We can perform the angular integral numerically by dividing up the celestial sphere into finite-size elements. We employed the Lebedev sparse-grid quadrature method [103]. We used the Lebedev rules on the unit sphere from the dataset directory `SPHERE_LEBEDEV_RULE`. For a chosen grid of points  $L_N = \{(\theta_i, \varphi_i)\}_{i=1}^P$  with associated weights  $W_i^{(N)}$  we write:

$$\int d\Omega f(\theta, \varphi) \simeq (4\pi) \sum_{\theta_i, \varphi_i \in L_N} W_i^{(N)}(\theta_i, \varphi_i) f(\theta_i, \varphi_i). \quad (\text{V.2})$$

We have used  $N = 17$ , corresponding to 110 points in  $L_N$ . The Lebedev rule of order  $N$  will integrate a spherical harmonic  $Y_{\ell m}(\theta, \phi)$  for  $\ell \leq N$  exactly.

### A. LO Power Spectrum

Using the tree-level waveform given in Appendix A, we can compute the LO flux as follows,

$$\frac{dE^{\text{LO}}}{d\omega} = \frac{2}{\kappa^2} \int d\Omega \omega^2 \sum_{h=\pm} |\mathcal{W}_h^{(0)}(\omega, \Omega)|^2. \quad (\text{V.3})$$

We can evaluate the flux numerically using the integrals in Eq. (A.12), and Lebedev quadrature for angular integrations. In Fig. 6 we show the relativistic spectrum computed numerically for different velocities. From the small-velocity expansion of the tree-level waveform instead, we can obtain an analytic result of the LO [ $\mathcal{O}(G^3)$ ] power spectrum in powers of  $p_\infty$ . In this limit, all frequency-domain integrals are reduced to the Bessel functions  $K_0(b\Omega), K_1(b\Omega)$ . We obtained an analytic expression for the LO spectrum up to order  $p_\infty^8$ , which is in agreement with previous results [43, 102].

### B. NLO Power Spectrum

We obtain the NLO contributions to the power spectrum from the interference of the LO and NLO frequency-

<sup>7</sup> The particular choice of the angular variable  $z$  corresponds to  $\theta \simeq \frac{\pi}{3}$  and  $\phi \simeq \frac{\pi}{3}$ .

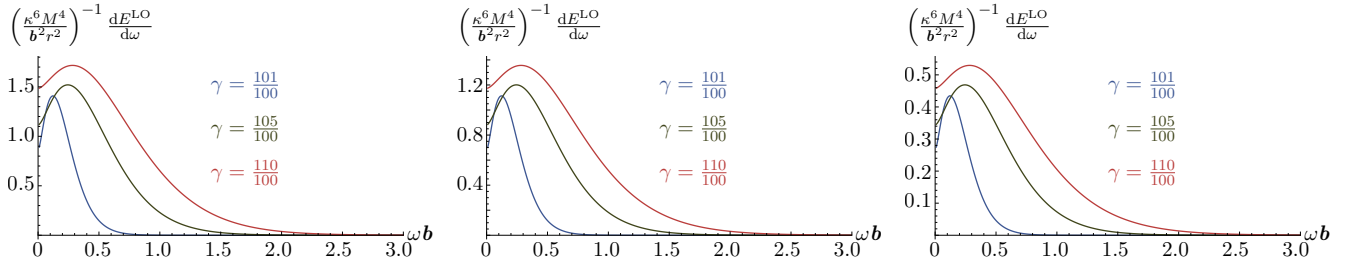


FIG. 6. Plots of the gravitational power spectrum at LO  $dE^{\text{LO}}/d\omega$  as a function of the energy  $\omega$ . Each plot shows different values of the boost  $\gamma$  with fixed symmetric mass ratios  $\nu$ , which are, respectively  $\{\frac{1}{4}, \frac{2}{9}, \frac{5}{36}\}$ .

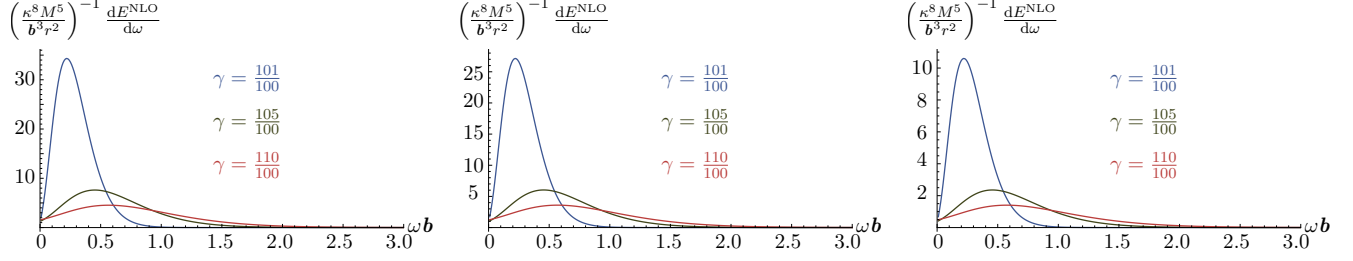


FIG. 7. Plots of the NLO corrections to the gravitational power spectrum  $dE^{\text{NLO}}/d\omega$  as a function of the energy  $\omega$ . Each plot shows different values of the boost  $\gamma$  with fixed symmetric mass ratios  $\nu$ , which are, respectively  $\{\frac{1}{4}, \frac{2}{9}, \frac{5}{36}\}$ .

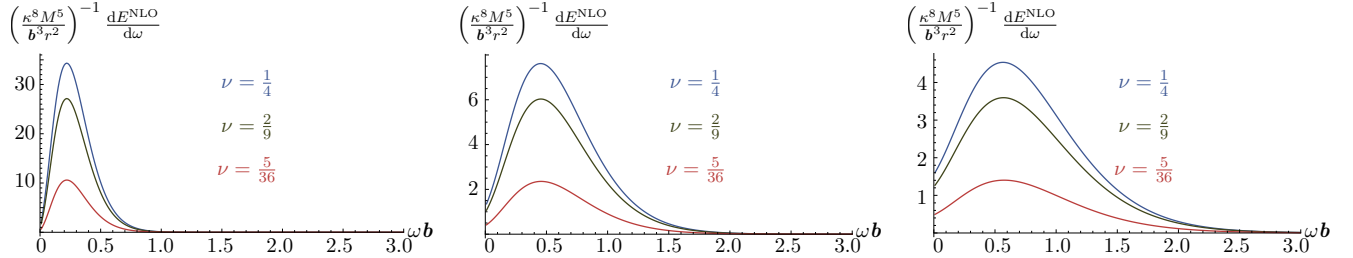


FIG. 8. Plots of the NLO corrections to the gravitational power spectrum  $dE^{\text{NLO}}/d\omega$  as a function of the energy  $\omega$ . Each plot shows different values of the symmetric mass ratio  $\nu$  with fixed values of the boost  $\gamma$ , which are, respectively  $\{\frac{101}{100}, \frac{105}{100}, \frac{110}{100}\}$ .

space waveforms,

$$\frac{dE^{\text{NLO}}}{d\omega} = \frac{2}{\kappa^2} \int d\Omega \omega^2 \sum_{h=\pm} [\mathcal{W}_h^{(1)} \mathcal{W}_h^{(0)*} + \mathcal{W}_h^{(0)} \mathcal{W}_h^{(1)*}]. \quad (\text{V.4})$$

In Figs. 7 8 we show the NLO power spectrum for different velocities and mass ratios.

## VI. CONCLUSIONS

In this article, we presented the first analytic expression for the gravitational waveform in impact-parameter space to next-to-leading order ( $\mathcal{O}(\kappa^{5/2})$ ) for scalar particles. We computed it directly from scattering amplitudes via the observables-based (KMOC) formalism. We treat Fourier and loop integrations on the same footing, which offers a novel strategy that extends unitarity-based integrand construction and integration-by-parts (IBP) reduc-

tion techniques to accommodate the Fourier exponential.

We evaluate the resulting integrals analytically, by combining canonical differential equations with a suitable contour deformation strategy. This hybrid method allows us to avoid spurious poles in the Fourier transform while maintaining analytic control over all master integrals contributing to the frequency-domain waveform.

We express the waveform in terms of a minimal basis of 28 combined master integrals. This set of integrals is not limited to emission from scalar scattering, but also suffices for emission from systems of spinning bodies.

We have verified that our results are consistent with those given previously in the literature [51–53, 55, 82] by separating infrared-divergent and tail contributions and confirmed agreement with known expressions in the small-velocity limit. We also evaluated the NLO power spectrum numerically, using Lebedev quadrature to integrate over the celestial sphere. Our results demonstrate the power of amplitude-based techniques in computing

classical observables and pave the way for further analytic studies of gravitational radiation at higher orders and including spin effects.

### ACKNOWLEDGMENTS

We would like to thank Lara Bohnenblust and Harald Ita for sharing the data of the plots in Ref. [55] for numerical comparison. SDA would like to thank Donato Bini and Thibault Damour for insightful discus-

sions, and Vincent He, Aidan Herderschee, Julio Parra-Martinez, Radu Roiban, and Fei Teng for collaborations on related projects. GB would like to thank Vsevolod Chestnov and Pierpaolo Mastrolia for valuable discussions. This research was supported by the European Research Council (ERC) under the European Union’s research and innovation program grant agreement ERC-AdG-885414 (‘Ampl2Einstein’). G.B. research is partially supported by the Italian MIUR under contract 20223ANFHR (PRIN2022), by the Università Italo-Francese, under grant Vinci, and by the Amplitudes INFN scientific initiative.

- 
- [1] G. Brunello and S. De Angelis, *JHEP* **07**, 062 (2024), [arXiv:2403.08009 \[hep-th\]](#).
  - [2] L. Blanchet and T. Damour, *Phil. Trans. Roy. Soc. Lond. A* **320**, 379 (1986).
  - [3] L. Blanchet and T. Damour, *Ann. Inst. H. Poincaré Phys. Theor.* **50**, 377 (1989).
  - [4] L. Blanchet, *Living Rev. Rel.* **17**, 2 (2014), [arXiv:1310.1528 \[gr-qc\]](#).
  - [5] W. D. Goldberger and I. Z. Rothstein, *Phys. Rev. D* **73**, 104029 (2006), [arXiv:hep-th/0409156](#).
  - [6] W. D. Goldberger and A. Ross, *Phys. Rev. D* **81**, 124015 (2010), [arXiv:0912.4254 \[gr-qc\]](#).
  - [7] S. Foffa and R. Sturani, *Class. Quant. Grav.* **31**, 043001 (2014), [arXiv:1309.3474 \[gr-qc\]](#).
  - [8] R. A. Porto, *Phys. Rept.* **633**, 1 (2016), [arXiv:1601.04914 \[hep-th\]](#).
  - [9] S. Foffa, P. Mastrolia, R. Sturani, and C. Sturm, *Phys. Rev. D* **95**, 104009 (2017), [arXiv:1612.00482 \[gr-qc\]](#).
  - [10] S. Foffa, R. A. Porto, I. Rothstein, and R. Sturani, *Phys. Rev. D* **100**, 024048 (2019), [arXiv:1903.05118 \[gr-qc\]](#).
  - [11] S. Foffa and R. Sturani, *Phys. Rev. D* **100**, 024047 (2019), [arXiv:1903.05113 \[gr-qc\]](#).
  - [12] J. Blümlein, A. Maier, P. Marquard, and G. Schäfer, *Nucl. Phys. B* **955**, 115041 (2020), [arXiv:2003.01692 \[gr-qc\]](#).
  - [13] S. Foffa, P. Mastrolia, R. Sturani, C. Sturm, and W. J. Torres Bobadilla, *Phys. Rev. Lett.* **122**, 241605 (2019), [arXiv:1902.10571 \[gr-qc\]](#).
  - [14] J. Blümlein, A. Maier, P. Marquard, and G. Schäfer, *Nucl. Phys. B* **983**, 115900 (2022), [Erratum: *Nucl. Phys. B* 985, 115991 (2022)], [arXiv:2110.13822 \[gr-qc\]](#).
  - [15] R. A. Porto, M. M. Riva, and Z. Yang, *JHEP* **04**, 050 (2025), [arXiv:2409.05860 \[gr-qc\]](#).
  - [16] Y. Iwasaki, *Prog. Theor. Phys.* **46**, 1587 (1971).
  - [17] T. Damour, *Phys. Rev. D* **94**, 104015 (2016), [arXiv:1609.00354 \[gr-qc\]](#).
  - [18] T. Damour, *Phys. Rev. D* **97**, 044038 (2018), [arXiv:1710.10599 \[gr-qc\]](#).
  - [19] C. Cheung, I. Z. Rothstein, and M. P. Solon, *Phys. Rev. Lett.* **121**, 251101 (2018), [arXiv:1808.02489 \[hep-th\]](#).
  - [20] N. E. J. Bjerrum-Bohr, P. H. Damgaard, G. Festuccia, L. Planté, and P. Vanhove, *Phys. Rev. Lett.* **121**, 171601 (2018), [arXiv:1806.04920 \[hep-th\]](#).
  - [21] Z. Bern, C. Cheung, R. Roiban, C.-H. Shen, M. P. Solon, and M. Zeng, *Phys. Rev. Lett.* **122**, 201603 (2019), [arXiv:1901.04424 \[hep-th\]](#).
  - [22] Z. Bern, C. Cheung, R. Roiban, C.-H. Shen, M. P. Solon, and M. Zeng, *JHEP* **10**, 206 (2019), [arXiv:1908.01493 \[hep-th\]](#).
  - [23] J. Parra-Martinez, M. S. Ruf, and M. Zeng, *JHEP* **11**, 023 (2020), [arXiv:2005.04236 \[hep-th\]](#).
  - [24] C. Cheung and M. P. Solon, *JHEP* **06**, 144 (2020), [arXiv:2003.08351 \[hep-th\]](#).
  - [25] P. Di Vecchia, C. Heissenberg, R. Russo, and G. Veneziano, *JHEP* **07**, 169 (2021), [arXiv:2104.03256 \[hep-th\]](#).
  - [26] A. Brandhuber, G. Chen, G. Travaglini, and C. Wen, *JHEP* **10**, 118 (2021), [arXiv:2108.04216 \[hep-th\]](#).
  - [27] G. Kälin, Z. Liu, and R. A. Porto, *Phys. Rev. Lett.* **125**, 261103 (2020), [arXiv:2007.04977 \[hep-th\]](#).
  - [28] G. Kälin and R. A. Porto, *JHEP* **11**, 106 (2020), [arXiv:2006.01184 \[hep-th\]](#).
  - [29] G. Mogull, J. Plefka, and J. Steinhoff, *JHEP* **02**, 048 (2021), [arXiv:2010.02865 \[hep-th\]](#).
  - [30] C. Dlapa, G. Kälin, Z. Liu, and R. A. Porto, *Phys. Lett. B* **831**, 137203 (2022), [arXiv:2106.08276 \[hep-th\]](#).
  - [31] Z. Bern, J. Parra-Martinez, R. Roiban, M. S. Ruf, C.-H. Shen, M. P. Solon, and M. Zeng, *Phys. Rev. Lett.* **126**, 171601 (2021), [arXiv:2101.07254 \[hep-th\]](#).
  - [32] Z. Bern, J. Parra-Martinez, R. Roiban, M. S. Ruf, C.-H. Shen, M. P. Solon, and M. Zeng, *PoS* **LL2022**, 051 (2022).
  - [33] C. Dlapa, G. Kälin, Z. Liu, J. Neef, and R. A. Porto, *Phys. Rev. Lett.* **130**, 101401 (2023), [arXiv:2210.05541 \[hep-th\]](#).
  - [34] G. U. Jakobsen, G. Mogull, J. Plefka, B. Sauer, and Y. Xu, *Phys. Rev. Lett.* **131**, 151401 (2023), [arXiv:2306.01714 \[hep-th\]](#).
  - [35] G. U. Jakobsen, G. Mogull, J. Plefka, and B. Sauer, *Phys. Rev. Lett.* **131**, 241402 (2023), [arXiv:2308.11514 \[hep-th\]](#).
  - [36] P. H. Damgaard, E. R. Hansen, L. Planté, and P. Vanhove, *JHEP* **09**, 183 (2023), [arXiv:2307.04746 \[hep-th\]](#).
  - [37] Z. Bern, E. Herrmann, R. Roiban, M. S. Ruf, A. V. Smirnov, V. A. Smirnov, and M. Zeng, *Phys. Rev. Lett.* **132**, 251601 (2024), [arXiv:2305.08981 \[hep-th\]](#).
  - [38] M. Driesse, G. U. Jakobsen, G. Mogull, J. Plefka, B. Sauer, and J. Usovitsch, *Phys. Rev. Lett.* **132**, 241402 (2024), [arXiv:2403.07781 \[hep-th\]](#).

- [39] Z. Bern, E. Herrmann, R. Roiban, M. S. Ruf, A. V. Smirnov, V. A. Smirnov, and M. Zeng, *JHEP* **10**, 023 (2024), arXiv:2406.01554 [hep-th].
- [40] M. Driesse, G. U. Jakobsen, A. Klemm, G. Mogull, C. Nega, J. Plefka, B. Sauer, and J. Usovitsch, *Nature* **641**, 603 (2025), arXiv:2411.11846 [hep-th].
- [41] T. Damour and P. Rettegnò, *Phys. Rev. D* **107**, 064051 (2023), arXiv:2211.01399 [gr-qc].
- [42] P. Rettegnò, G. Pratten, L. M. Thomas, P. Schmidt, and T. Damour, *Phys. Rev. D* **108**, 124016 (2023), arXiv:2307.06999 [gr-qc].
- [43] G. U. Jakobsen, G. Mogull, J. Plefka, and J. Steinhoff, *Phys. Rev. Lett.* **126**, 201103 (2021), arXiv:2101.12688 [gr-qc].
- [44] S. Mougiakakos, M. M. Riva, and F. Vernizzi, *Phys. Rev. D* **104**, 024041 (2021), arXiv:2102.08339 [gr-qc].
- [45] G. U. Jakobsen, G. Mogull, J. Plefka, and J. Steinhoff, *Phys. Rev. Lett.* **128**, 011101 (2022), arXiv:2106.10256 [hep-th].
- [46] S. De Angelis, P. P. Novichkov, and R. Gonzo, *Phys. Rev. D* **110**, L041502 (2024), arXiv:2309.17429 [hep-th].
- [47] A. Brandhuber, G. R. Brown, G. Chen, J. Gowdy, and G. Travaglini, *JHEP* **02**, 026 (2024), arXiv:2310.04405 [hep-th].
- [48] R. Aoude, K. Haddad, C. Heissenberg, and A. Helset, *Phys. Rev. D* **109**, 036007 (2024), arXiv:2310.05832 [hep-th].
- [49] D. A. Kosower, B. Maybee, and D. O’Connell, *JHEP* **02**, 137 (2019), arXiv:1811.10950 [hep-th].
- [50] A. Cristofoli, R. Gonzo, D. A. Kosower, and D. O’Connell, *Phys. Rev. D* **106**, 056007 (2022), arXiv:2107.10193 [hep-th].
- [51] A. Brandhuber, G. R. Brown, G. Chen, S. De Angelis, J. Gowdy, and G. Travaglini, *JHEP* **06**, 048 (2023), arXiv:2303.06111 [hep-th].
- [52] A. Herderschee, R. Roiban, and F. Teng, *JHEP* **06**, 004 (2023), arXiv:2303.06112 [hep-th].
- [53] A. Georgoudis, C. Heissenberg, and I. Vazquez-Holm, *JHEP* **06**, 126 (2023), arXiv:2303.07006 [hep-th].
- [54] S. Caron-Huot, M. Giroux, H. S. Hannesdottir, and S. Mizera, *JHEP* **01**, 139 (2024), arXiv:2308.02125 [hep-th].
- [55] L. Bohnenblust, H. Ita, M. Kraus, and J. Schlenk, *JHEP* **11**, 109 (2024), arXiv:2312.14859 [hep-th].
- [56] Z. Bern, L. J. Dixon, D. C. Dunbar, and D. A. Kosower, *Nucl. Phys. B* **425**, 217 (1994), arXiv:hep-ph/9403226.
- [57] Z. Bern, L. J. Dixon, D. C. Dunbar, and D. A. Kosower, *Nucl. Phys. B* **435**, 59 (1995), arXiv:hep-ph/9409265.
- [58] R. Britto, F. Cachazo, and B. Feng, *Nucl. Phys. B* **725**, 275 (2005), arXiv:hep-th/0412103.
- [59] R. Britto, B. Feng, and P. Mastrolia, *Phys. Rev. D* **73**, 105004 (2006), arXiv:hep-ph/0602178.
- [60] G. Ossola, C. G. Papadopoulos, and R. Pittau, *Nucl. Phys. B* **763**, 147 (2007), arXiv:hep-ph/0609007.
- [61] C. Anastasiou, R. Britto, B. Feng, Z. Kunszt, and P. Mastrolia, *JHEP* **03**, 111 (2007), arXiv:hep-ph/0612277.
- [62] A. Brandhuber, G. Chen, G. Travaglini, and C. Wen, *JHEP* **07**, 047 (2021), arXiv:2104.11206 [hep-th].
- [63] F. V. Tkachov, *Phys. Lett. B* **100**, 65 (1981).
- [64] K. G. Chetyrkin and F. V. Tkachov, *Nucl. Phys. B* **192**, 159 (1981).
- [65] S. Laporta, *Int. J. Mod. Phys. A* **15**, 5087 (2000), arXiv:hep-ph/0102033.
- [66] A. V. Smirnov, *JHEP* **10**, 107 (2008), arXiv:0807.3243 [hep-ph].
- [67] R. N. Lee, (2012), arXiv:1212.2685 [hep-ph].
- [68] P. Maierhöfer, J. Usovitsch, and P. Uwer, *Comput. Phys. Commun.* **230**, 99 (2018), arXiv:1705.05610 [hep-ph].
- [69] T. Peraro, *JHEP* **07**, 031 (2019), arXiv:1905.08019 [hep-ph].
- [70] Z. Wu, J. Boehm, R. Ma, H. Xu, and Y. Zhang, *Comput. Phys. Commun.* **295**, 108999 (2024), arXiv:2305.08783 [hep-ph].
- [71] K. Matsumoto, *Funkcial. Ekvac.* **41**, 291 (1998).
- [72] H. Majima, K. Matsumoto, and N. Takayama, *Tohoku Math. J. (2)* **52**, 489 (2000).
- [73] S. L. Cacciatori and P. Mastrolia, (2022), arXiv:2211.03729 [hep-th].
- [74] G. Brunello, G. Crisanti, M. Giroux, P. Mastrolia, and S. Smith, *Phys. Rev. D* **109**, 094047 (2024), arXiv:2311.14432 [hep-th].
- [75] D. A. Kosower, R. Monteiro, and D. O’Connell, *J. Phys. A* **55**, 443015 (2022), arXiv:2203.13025 [hep-th].
- [76] J. S. Schwinger, *J. Math. Phys.* **2**, 407 (1961).
- [77] L. V. Keldysh, *Zh. Eksp. Teor. Fiz.* **47**, 1515 (1964).
- [78] G. U. Jakobsen, G. Mogull, J. Plefka, and B. Sauer, *JHEP* **10**, 128 (2022), arXiv:2207.00569 [hep-th].
- [79] G. Kälin, J. Neef, and R. A. Porto, *JHEP* **01**, 140 (2023), arXiv:2207.00580 [hep-th].
- [80] G. Veneziano and G. A. Vilkovisky, *Phys. Lett. B* **834**, 137419 (2022), arXiv:2201.11607 [gr-qc].
- [81] A. Georgoudis, C. Heissenberg, and R. Russo, *JHEP* **03**, 089 (2024), arXiv:2312.07452 [hep-th].
- [82] D. Bini, T. Damour, S. De Angelis, A. Geralico, A. Herderschee, R. Roiban, and F. Teng, *Phys. Rev. D* **109**, 125008 (2024), arXiv:2402.06604 [hep-th].
- [83] P. H. Damgaard, K. Haddad, and A. Helset, *JHEP* **11**, 070 (2019), arXiv:1908.10308 [hep-ph].
- [84] N. E. J. Bjerrum-Bohr, L. Planté, and P. Vanhove, *JHEP* **03**, 071 (2022), arXiv:2111.02976 [hep-th].
- [85] Z. Bern and D. A. Kosower, *Nucl. Phys. B* **379**, 451 (1992).
- [86] W. Siegel, *Phys. Lett. B* **84**, 193 (1979).
- [87] C. Anastasiou, J. Karlen, and M. Vicini, *JHEP* **12**, 169 (2023), arXiv:2308.14701 [hep-ph].
- [88] P. Mastrolia and S. Mizera, *JHEP* **02**, 139 (2019), arXiv:1810.03818 [hep-th].
- [89] G. Brunello, V. Chestnov, G. Crisanti, H. Frellesvig, M. K. Mandal, and P. Mastrolia, *JHEP* **09**, 015 (2024), arXiv:2401.01897 [hep-th].
- [90] C. Anastasiou and K. Melnikov, *Nucl. Phys. B* **646**, 220 (2002), arXiv:hep-ph/0207004.
- [91] C. Anastasiou, K. Melnikov, and F. Petriello, *Phys. Rev. D* **69**, 076010 (2004), arXiv:hep-ph/0311311.
- [92] E. Herrmann, J. Parra-Martinez, M. S. Ruf, and M. Zeng, *Phys. Rev. Lett.* **126**, 201602 (2021), arXiv:2101.07255 [hep-th].
- [93] S. De Angelis, D. A. Kosower, R. Ma, Z. Wu, and Y. Zhang, (2025), arXiv:2508.04394 [hep-th].
- [94] L. Blanchet and T. Damour, *Phys. Rev. D* **37**, 1410 (1988).
- [95] S. Weinberg, *Phys. Rev.* **140**, B516 (1965).
- [96] D. Bini, T. Damour, and A. Geralico, *Phys. Rev. D* **108**, 124052 (2023), arXiv:2309.14925 [gr-qc].
- [97] B. J. Owen and B. S. Sathyaprakash, *Phys. Rev. D* **60**, 022002 (1999), arXiv:gr-qc/9808076.

- [98] L. Blanchet and G. Schaefer, *Class. Quant. Grav.* **10**, 2699 (1993).
- [99] L. Bohnenblust, H. Ita, M. Kraus, and J. Schlenk, (2025), [arXiv:2505.15724 \[hep-th\]](#).
- [100] A. Elkhidir, D. O'Connell, and R. Roiban, *Phys. Rev. Lett.* **135**, 151601 (2025), [arXiv:2408.15961 \[hep-th\]](#).
- [101] G. Brunello, V. Chestnov, G. Crisanti, M. Giroux, and S. Smith, (2025), [arXiv:2510.26874 \[hep-th\]](#).
- [102] D. Bini and T. Damour, *Phys. Rev. D* **110**, 064005 (2024), [arXiv:2406.04878 \[gr-qc\]](#).
- [103] V. Lebedev, *USSR Computational Mathematics and Mathematical Physics* **16**, 10 (1976).
- [104] S. J. Kovacs and K. S. Thorne, *Astrophys. J.* **224**, 62 (1978).
- [105] M. Besier, P. Wasser, and S. Weinzierl, *Comput. Phys. Commun.* **253**, 107197 (2020), [arXiv:1910.13251 \[cs.MS\]](#).
- [106] M. M. Riva and F. Vernizzi, *JHEP* **11**, 228 (2021), [arXiv:2110.10140 \[hep-th\]](#).

## Appendix A: The LO Waveform

Here we present an analytic derivation of the LO gravitational waveform in the frequency domain. The derivation illustrates the main features of the framework that underpins our one-loop computation. At this order, the waveform receives contributions only from tree-level amplitudes. The result was originally obtained in the time domain by Kovacs and Thorne [104], and more recently using WQFT [43–45] and QFT techniques [46–48].

*a. Integrand and Generalized Unitarity.* We can construct the integrand for the tree-level amplitude using generalized unitarity cuts in the  $q_i^2$  channels. In this case each of these cuts correspond to a single on-shell graviton exchange, as shown in Fig. 9,

$$T^{(0)} = \text{Cut}_{[q_2]}[\mathcal{M}_4^{(0)}(\bar{p}_1; -q_2, k) \otimes_1 \mathcal{M}_3^{(0)}(\bar{p}_2; q_2)] \cup \text{Cut}_{[q_1]}[\mathcal{M}_3^{(0)}(\bar{p}_1; q_1) \otimes_1 \mathcal{M}_4^{(0)}(\bar{p}_2; -q_1, k)]. \quad (\text{A.1})$$

The symbol  $\otimes_i$  denotes the sewing of  $i$  internal graviton lines, and  $\text{Cut}_{[j]}$  indicates the generalized unitarity cut in the  $[j]$  legs. The symbol  $\cup$  stands for the merging the contributions of the two factorization channels; this is necessary to avoid double counting contributions which have non-vanishing residues at both  $q_1^2 = 0$  and  $q_2^2 = 0$ . The three-point amplitudes we need to build the integrand are,

$$\mathcal{M}_3^{(0)}(p_i; k) = \kappa(\varepsilon_k \cdot p_i)^2, \quad \mathcal{M}_3^{(0)}(k_1, k_2, k_3) = \kappa(\varepsilon_1 \cdot \varepsilon_2 \varepsilon_3 \cdot k_1 + \varepsilon_2 \cdot \varepsilon_3 \varepsilon_1 \cdot k_2 + \varepsilon_3 \cdot \varepsilon_1 \varepsilon_2 \cdot k_3)^2, \quad (\text{A.2})$$

written in a double-copy form. From these amplitudes we can build the quantum Compton amplitude,

$$\mathcal{M}_4^{(0)}(p_i \rightarrow p'_i, k_1, k_2) = \kappa^2 \frac{(p_i \cdot F_1 \cdot F_2 \cdot p_i + p'_i \cdot F_1 \cdot F_2 \cdot p'_i)^2}{(2k_1 \cdot k_2)(2p_i \cdot k_1)(2p_i \cdot k_2)}, \quad (\text{A.3})$$

where the vector-field strength tensor is  $F_i^{\mu\nu} = k_i^\mu \varepsilon_i^\nu - k_i^\nu \varepsilon_i^\mu$  and the Riemann tensor can be built out of it using a double copy:  $R_i^{\mu\nu\rho\sigma} = F_i^{\mu\nu} F_i^{\rho\sigma}$ . We expand the Compton amplitude in the heavy-mass limit,

$$\mathcal{M}_4^{(0)}(\bar{p}_i; k_1 k_2) = \kappa^2 \left[ i\pi \bar{m}_i^3 \delta(\bar{u}_i \cdot k_1) (\varepsilon_{k_1} \cdot \bar{u}_i)^2 (\varepsilon_{k_2} \cdot \bar{u}_i)^2 - \bar{m}_i^2 \frac{(\bar{u}_i \cdot F_1 \cdot F_2 \cdot \bar{u}_i)^2}{(k_1 \cdot \bar{u}_i)^2 q^2} \right], \quad (\text{A.4})$$

where as in Eq. (II.15) we have expanded around  $\bar{p}_i^\mu = \bar{m}_i \bar{u}_i^\mu = p_i^\mu + \frac{q^\mu}{2}$ , with  $q^\mu = k_1^\mu + k_2^\mu$ ,  $\bar{u}_i^2 = 1$  and  $\bar{u}_i \cdot q = 0$ , as prescribed by the LIPS measure (II.10). After summing over the internal graviton helicities using Eq. (III.2) and combining the various cuts, the integrand is,

$$T^{(0)} = \frac{m_1^2 m_2^2 \kappa^3}{q_1^2 q_2^2 w_1^2} \left[ (q_1 \cdot F_k \cdot u_1)^2 \left( y^2 - \frac{1}{D_s - 2} \right) + \frac{q_1 \cdot F_k \cdot u_1 u_1 \cdot F_k \cdot u_2}{w_2} \left( -y(q_2^2 + 2w_1 w_2) + \frac{1}{D_s - 2} q_2^2 \right) \right. \\ \left. + \frac{(u_1 \cdot F_k \cdot u_2)^2}{4w_2^2} \left( (q_2^2 y + 2w_1 w_2)^2 - \frac{1}{D_s - 2} q_2^4 \right) \right], \quad (\text{A.5})$$

where  $D_s - 2$  is the number of graviton spin degrees of freedom in the chosen variant of dimensional regularization.

*b. Integrand reduction* The frequency space LO waveform (II.9) is given by the Fourier transform of the tree-level integrand (A.1),

$$\mathcal{W}_h^{(0)}(\omega, \hat{\mathbf{n}}) = \kappa \frac{e^{i\omega n \cdot b_2}}{4\pi r} \int_{\hat{q}} \hat{\delta}(2m_1 u_1 \cdot q) \hat{\delta}(2m_2 u_2 \cdot (k - q)) e^{ib \cdot q} T^{(0)}. \quad (\text{A.6})$$

Here,  $n^\mu = (1, \hat{\mathbf{n}})$ . We want to treat this object as a generalized one-loop integral. We can decompose the ‘tensor’ numerators of the form  $q_1 \cdot F_k \cdot u_1$  in terms of form factors. The required form factor can be obtained from the generic rank- $N$  relation presented in Appendix D. The scalar integrals present in the form factors then belong to a single generalized integral family, of the form,

$$I_{a_1 1 1 a_4 a_5} = \int_{\hat{q}} \frac{e^{D_{t:1}} \hat{\delta}(D_{t:2}) \hat{\delta}(D_{t:3}) D_{t:1}^{-a_1}}{D_{t:4}^{a_4} D_{t:5}^{a_5}}. \quad (\text{A.7})$$

The invariants  $D_{t:i}$  are defined as follows,

$$D_{t:1} = i q \cdot b, \quad D_{t:2} = \bar{u}_1 \cdot q, \quad D_{t:3} = \bar{u}_2 \cdot (k - q), \quad D_{t:4} = q^2, \quad D_{t:5} = (q - k)^2. \quad (\text{A.8})$$

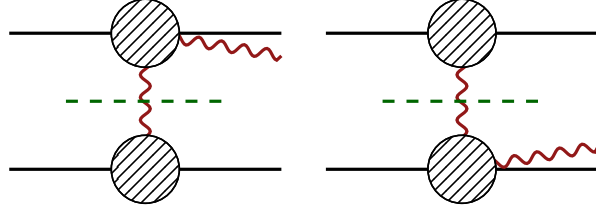


FIG. 9. The singularities in the  $q_i^2$  channels are probed by generalized unitarity cuts in complex kinematics. At tree-level we have contributions only from the one-graviton exchange.

Just as for the integrals discussed in main text, relations between these integrals arise from generalized IBP relations, here effectively in  $q$ -space,

$$\int_{\hat{q}} \frac{\partial}{\partial q^\mu} \left( \frac{v^\mu e^{D_{t1}}}{\prod_{i=1}^5 D_{t;i}^{\alpha_i}} \right) = 0. \quad (\text{A.9})$$

Here the relations allow us to rewrite the LO waveform in terms of just six Fourier MIs, of which three are base integrals and three are ‘derivative’ integrals. (As in the text, the latter may be obtained from the former by taking a derivative with respect to the impact parameter  $b$ .) The basis integrals are,

$$J_1 = I_{01110}, \quad J_2 = \underline{I}_{-11110}, \quad J_3 = I_{01101}, \quad J_4 = \underline{I}_{-11101}, \quad J_5 = I_{01111}, \quad J_6 = \underline{I}_{-11111}. \quad (\text{A.10})$$

The waveform can be written as a linear combination of these integrals,

$$\mathcal{W}_h^{(0)}(\omega, \hat{\mathbf{n}}) = \sum_{i=1}^6 c_i J_i, \quad (\text{A.11})$$

where the coefficients  $c_i$  are rational functions of the kinematic invariants; we give their expressions in the ancillary file `coefficients_tree.m`.

*c. Integration.* Analytic expressions for the MIs can be obtained from the general results in Appendix F, obtained via Schwinger parametrization, Eqs. (F.25), by setting  $\alpha_1 = \alpha_2 = 1$ . For completeness, we also present expressions for the MIs in  $D = 4$  obtained using the contour deformation method explained in Appendix F. In this case, the complex structure in the  $z_v$  plane is simpler. The integrands contain only poles corresponding to  $q_1^2 = 0$  and  $q_2^2 = 0$  [46], as shown in Fig. 10. Performing the  $z_v$  integration by contour deformation we obtain,

$$\begin{aligned} J_1 &= -\frac{1}{4\pi \bar{m}_1 \bar{m}_2 \sqrt{\gamma^2 - 1}} \int_{-\infty}^{+\infty} dz_b e^{-ibz_b} \frac{1}{\sqrt{z_b^2 + \hat{w}_2^2}}, \\ J_3 &= -\frac{1}{4\pi \bar{m}_1 \bar{m}_2 \sqrt{\gamma^2 - 1}} \int_{-\infty}^{+\infty} dz_b e^{-ibz_b} \frac{1}{\sqrt{(b \cdot k/\mathbf{b} + z_b)^2 + \hat{w}_1^2}}, \\ J_5 &= \frac{1}{4\pi \bar{m}_1 \bar{m}_2 \sqrt{\gamma^2 - 1}} \int_{-\infty}^{+\infty} dz_b e^{-ibz_b} \frac{[(b \cdot k/\mathbf{b} + z_b)^2 + \hat{w}_1^2]^{-1/2} + [z_b^2 + \hat{w}_2^2]^{-1/2}}{(b \cdot k/\mathbf{b})^2 + \left[ \sqrt{z_b^2 + \hat{w}_2^2} + \sqrt{(b \cdot k/\mathbf{b} + z_b)^2 + \hat{w}_1^2} \right]^2}. \end{aligned} \quad (\text{A.12})$$

The  $z_b$  integrals can then be evaluated numerically after contour deformation.

*d. Time domain.* Starting from the frequency-space waveform, we can obtain the time-domain one as in Eq. (II.8). It suffices to rescale  $z_b$  and re-express  $k^\mu$ ,

$$z_b \rightarrow \omega \bar{z}_b, \quad k^\mu \rightarrow \omega n^\mu, \quad (\text{A.13})$$

to see that the overall dependence of the amplitude is  $\mathcal{W}_h^{(0)}(\omega, \hat{\mathbf{n}}) \sim \omega^0$ . As a result, we can combine the two exponentials to form a delta function, rendering the transformation to the time domain trivial,

$$J_i(t) = \int \hat{d}\omega e^{-i\omega u} J_i(\omega) = f_i(\bar{z}_b) \Big|_{\bar{z}_b \rightarrow -u/\sqrt{-b^2}}, \quad (\text{A.14})$$

with  $u = t - r$  the retarded time, just as in the main text.

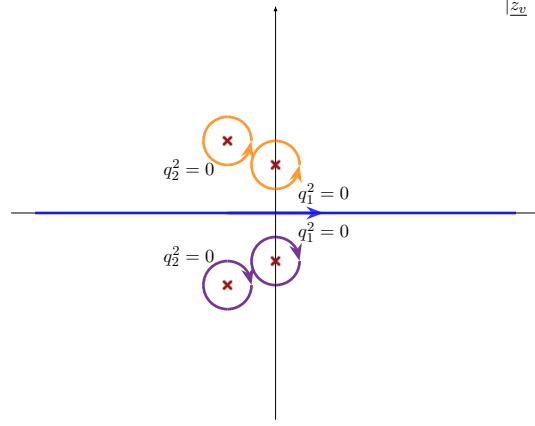


FIG. 10. The analytic structure of the  $z_v$  integrals appearing in the LO waveform. In general, each integral has four poles corresponding to the configurations in which  $q_1^2 = 0$  and  $q_2^2 = 0$ . We can apply Cauchy's residue theorem to deform the integration contour in the upper- or lower-half plane in order to have it wrap around the poles. This simplifies the computation to a sum of residues.

### Appendix B: The One-Loop Gravitational Compton Amplitude

The one-loop gravitational Compton integrand can be reconstructed from its generalized unitarity cuts (see Fig. 4) in the  $(\bar{p}_i, k_1)$  channel and in the  $q$  channel (the expression in the  $(\bar{p}_i, k_2)$  channel can be obtained by exchanging  $k_1 \leftrightarrow k_2$ ), as:

$$\mathcal{M}_4^{(1)}(\bar{p}_i; k_1, k_2) = \mathcal{C}_{\bar{p}_i, k_1} \cup \mathcal{C}_{\bar{p}_i, k_2} \cup \mathcal{C}_q, \quad (\text{B.1})$$

where  $\mathcal{C}_i$  denotes the contribution from the cut in the  $i$  channel, and the symbol  $\cup$  stands for the merging of the contributions. The ingredients are the tree-level Compton amplitude, in Eq. (A.3), and the four-graviton amplitude:

$$\mathcal{M}_4^{(0)}(k_1, k_2, k_3, k_4) = \kappa^2 \frac{(F_1 \cdot F_2 \cdot F_3 \cdot F_4 - F_1 \cdot F_2 F_3 \cdot F_4/4 + (3 \leftrightarrow 4) + (2 \leftrightarrow 3))^2}{(2k_1 \cdot k_2)(2k_2 \cdot k_3)(2k_1 \cdot k_3)}. \quad (\text{B.2})$$

The  $(\bar{p}_i, k_1)$  cut is obtained by gluing two tree-level Compton amplitudes at order  $\bar{m}_i^2$ :

$$\begin{aligned} \mathcal{M}_4^{(1)}(\bar{p}_i; k_1, k_2) \Big|_{(\bar{p}_i, k_1)} &= \kappa^4 \bar{m}_i^3 \left[ - \left( 1 - \frac{1}{D_s - 2} \right) \frac{\bar{u}_i \cdot F_{1, \mu_1} \bar{u}_i \cdot F_{1, \mu_2} \bar{u}_i \cdot F_{2, \mu_3} \bar{u}_i \cdot F_{2, \mu_4}}{(\bar{u}_i \cdot k_1)^4} I_{1,1,1,1}^{0; \mu_1 \mu_2 \mu_3 \mu_4} \Big|_{(\bar{p}_i, k_1)} \right. \\ &\quad + 2 \bar{u}_i \cdot F_1 \cdot F_2 \cdot \bar{u}_i \frac{\bar{u}_i \cdot F_{1, \mu_1} \bar{u}_i \cdot F_{1, \mu_2}}{(\bar{u}_i \cdot k_1)^2} I_{1,1,1,1}^{0; \mu_1 \mu_2} \Big|_{(\bar{p}_i, k_1)} \\ &\quad \left. - (\bar{u}_i \cdot F_1 \cdot F_2 \cdot \bar{u}_i)^2 I_{1,1,1,1}^{0;} \Big|_{(\bar{p}_i, k_1)} \right], \end{aligned} \quad (\text{B.3})$$

where  $\Big|_{(\bar{p}_i, k_1)}$  denotes the cut in the  $(\bar{p}_i, k_1)$  channel, and,

$$I_{1,1,1,1}^{0; \mu_1 \dots \mu_n} = \int_{\hat{\ell}} \ell^{\mu_1} \dots \ell^{\mu_n} \frac{i\pi \delta((\ell + k_1) \cdot \bar{u}_i)}{(k_1 + \ell)^2 \ell^2 (\ell - k_2)^2}. \quad (\text{B.4})$$

The  $q$ -channel cut is obtained instead by sewing the Compton amplitude at order  $\bar{m}_i^3$  with the four-graviton

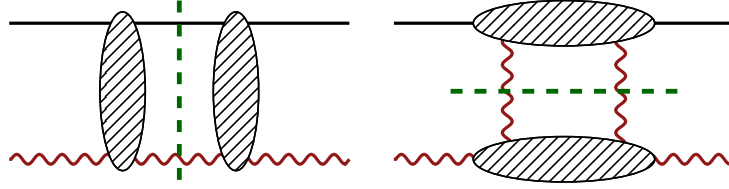


FIG. 11. Generalized unitarity cuts in the  $(\bar{p}, k_1)$  and  $q$  channels used to reconstruct the one-loop gravitational Compton integrand; the  $(\bar{p}, k_2)$  cut can be obtained by exchanging  $k_1 \leftrightarrow k_2$ .

amplitude, and is given by:

$$\begin{aligned}
\mathcal{M}_4^{(1)}(\bar{p}_i; k_1, k_2) \Big|_q &= \kappa^4 \bar{m}_i^3 \left\{ - \left( 1 - \frac{1}{D_s - 2} \right) \frac{4F_{1\mu_1} \cdot F_{2\mu_2} F_{1\mu_3} \cdot F_{2\mu_4}}{q^4} I_{1,1,1,1}^{1;\mu_1\mu_2\mu_3\mu_4} \Big|_{(q)} \right. \\
&\quad - \frac{2(\bar{u}_i \cdot F_{2,\mu_1})(k_2 \cdot F_1 \cdot \bar{u}_i F_{1\mu_2} \cdot F_{2\mu_3} - k_2 \cdot F_{1\mu_2} F_{1\mu_3} \cdot F_2 \cdot \bar{u}_i)}{(D_s - 2)q^4} I_{1,1,1,1}^{1;\mu_1\mu_2\mu_3} \Big|_{(q)} \\
&\quad - \frac{1}{4(D_s - 2)q^4} \left[ 8F_{1\mu_1} \cdot F_{2\mu_2} (2(D_s - 2) - 5)q^2 \bar{u}_i \cdot F_1 \cdot F_2 \cdot \bar{u}_i - 4k_1 \cdot F_2 \cdot \bar{u}_i k_2 \cdot F_1 \cdot \bar{u}_i \right. \\
&\quad + 2k_1 \cdot \bar{u}_i (5k_2 \cdot F_{1\mu_1} F_{2\mu_2} \cdot \bar{u}_i - 6k_1 \cdot F_{2\mu_1} F_{1\mu_2} \cdot \bar{u}_i) \\
&\quad + 4k_2 \cdot F_{1\mu_1} k_1 \cdot F_2 \cdot \bar{u}_i (4F_{1\mu_2} \cdot F_2 \cdot \bar{u}_i - 3F_{2\mu_2} \cdot F_1 \cdot \bar{u}_i) \\
&\quad + 8q^2 (F_{1\mu_1} \cdot F_2 \cdot \bar{u}_i F_{1\mu_2} \cdot F_2 \cdot \bar{u}_i + 3F_{2\mu_1} \cdot F_1 \cdot \bar{u}_i F_{1\mu_2} \cdot F_2 \cdot \bar{u}_i + F_{2\mu_1} \cdot F_1 \cdot \bar{u}_i F_{2\mu_2} \cdot F_1 \cdot \bar{u}_i) \\
&\quad - 8k_1 \cdot F_{2,\mu_1} (k_2 \cdot F_1 \cdot \bar{u}_i (F_{1\mu_2} \cdot F_2 \cdot \bar{u}_i - 2 \cdot F_{2\mu_2} \cdot F_1 \cdot \bar{u}_i) + k_2 \cdot F_{1,\mu_2} \bar{u}_i \cdot F_1 \cdot F_2 \cdot \bar{u}_i) \\
&\quad \left. - 5q^2 F_{1\mu_1} \cdot \bar{u}_i F_{2\mu_2} \cdot \bar{u}_i \right] I_{1,1,1,1}^{1;\mu_1\mu_2} \Big|_{(q)} \\
&\quad - \frac{\text{Tr}[F_1 \cdot F_2]}{4(D_s - 2)q^2} \left[ 2k_1 \cdot \bar{u}_i (F_{1\mu_1} \cdot F_2 \cdot \bar{u}_i - F_{2\mu_1} \cdot F_1 \cdot \bar{u}_i) \right. \\
&\quad \left. + F_{1\mu_1} \cdot \bar{u}_i k_1 \cdot F_2 \cdot \bar{u}_i - 6F_{2\mu_1} \cdot \bar{u}_i k_2 \cdot F_1 \cdot \bar{u}_i \right] I_{1,1,1,1}^{1;\mu_1} \Big|_{(q)} \\
&\quad \left( \frac{3\text{Tr}[F_1 \cdot F_2] \bar{u}_i \cdot F_1 \cdot F_2 \cdot \bar{u}_i}{4(D_s - 2)} - (\bar{u}_i \cdot F_1 \cdot F_2 \cdot \bar{u}_i)^2 \right) I_{1,1,1,1}^1 \Big|_{(q)} \\
&\quad \left. + (1 \leftrightarrow 2) \right\}, \tag{B.5}
\end{aligned}$$

where the integral families  $I_{1,1,1,1}^{1;\mu_1 \dots \mu_n}$ ,  $I_{1,1,1,1}^{2;\mu_1 \dots \mu_n}$  are defined as,

$$I_{1,1,1,1}^{1;\mu_1 \dots \mu_n} = \int_{\hat{\ell}} \ell^{\mu_1} \dots \ell^{\mu_n} \frac{i\pi \delta(\ell \cdot \bar{u}_i)}{(\ell)^2 (\ell + k_1)^2 (\ell + q)^2}, \quad I_{1,1,1,1}^{2;\mu_1 \dots \mu_n} = \int_{\hat{\ell}} \ell^{\mu_1} \dots \ell^{\mu_n} \frac{i\pi \delta(\ell \cdot \bar{u}_i)}{(\ell)^2 (\ell + k_2)^2 (\ell + q)^2}. \tag{B.6}$$

Here,  $(1 \leftrightarrow 2)$  is the crossed term obtained by exchanging  $k_1$  and  $k_2$  (and their polarizations), wherein the loop integrals are those of the  $I_{1,1,1,1}^{2;\mu_1 \dots \mu_n}$  family.

To avoid double counting of contributions with non-vanishing residues in more than one channel, the three generalized cuts must be merged at the integrand level. We proceed by building a permutation-symmetric, gauge-invariant ansatz composed of all independent tensor structures up to rank four, containing exactly four linearized field-strength tensors (two  $F_1$  and two  $F_2$ ), contracted with  $\{k_1, k_2, \ell, \bar{u}_i\}$ . The scalar denominator factors are organized into three structures, corresponding to different trivalent graphs, given by:

$$\mathcal{D}_1 = \ell^2 (\ell + k_1)^2 (\ell + q)^2, \quad \mathcal{D}_2 = \ell^2 (\ell + k_2)^2 (\ell + q)^2, \quad \mathcal{D}_3 = \ell^2 (\ell + q)^2. \tag{B.7}$$

Redundancies are eliminated using Bianchi identities, momentum conservation, and imposing symmetry under  $k_1 \leftrightarrow k_2$  exchange. The remaining undetermined coefficients—rational functions of the external kinematic invariants—are then fixed by imposing the simultaneous matching of the  $(\bar{p}, k_1)$ ,  $(\bar{p}, k_2)$  and  $q$ -channel cuts, yielding a unique non-redundant integrand.

The final compact expression for the one-loop Compton amplitude in the classical limit is provided in the ancillary file `compton.m`.

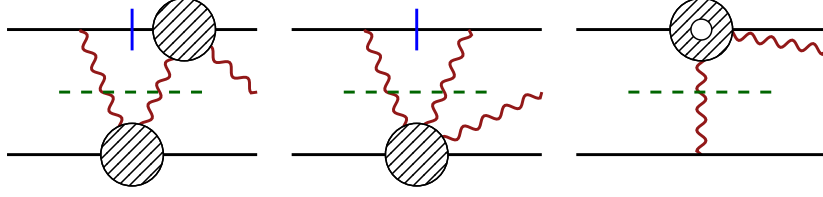


FIG. 12. The three generalized unitarity cuts yielding the  $\bar{m}_1^3 \bar{m}_2^2$  contribution to the one-loop waveform integrand. Blobs denote tree-level amplitudes in the heavy-mass expansion; the one-loop classical Compton subdiagram contains a single localized (delta-function) matter propagator.

### Appendix C: Merging Generalized Cuts for the One-Loop Gravitational Waveform

The one-loop integrand for the gravitational waveform is obtained by consistently merging the generalized unitarity cut contributions shown in Fig. 1, together with the analogous terms generated by exchanging the two massive lines. The integrand is given by,

$$T^{(1)} = \text{Cut}_{[\ell, \ell - q_2]} [\mathcal{M}_5^{(0)}(\bar{p}_1; -\ell, \ell - q_2, k) \otimes_2 \mathcal{M}_4^{(0)}(\bar{p}_2; \ell, -\ell + q_2)] \cup \text{Cut}_{[q_2]} [\mathcal{M}_4^{(1)}(\bar{p}_1; -q_2, k) \otimes_1 \mathcal{M}_3^{(0)}(\bar{p}_2; q_2)] + (1 \leftrightarrow 2), \quad (\text{C.1})$$

where  $(1 \leftrightarrow 2)$  denotes the exchange of the two massive lines. As in Appendix A, the operator  $\otimes_i$  denotes sewing across  $i$  on-shell internal graviton lines, and  $\text{Cut}_{[j]}$  denotes the generalized unitarity cut in the denominators  $[j]$ . The required building blocks are: the one-loop Compton amplitude (Appendix B); the tree-level five-point amplitude [62]; and the tree-level four-point amplitude in Eq. (A.4). In the heavy-mass expansion, classical one-loop contributions scale as  $\bar{m}_1^3 \bar{m}_2^2$  and  $\bar{m}_1^2 \bar{m}_2^3$ . The  $\bar{m}_1^3 \bar{m}_2^2$  term (Fig. 12) expressed in terms of classical amplitudes reads:

$$T^{(1)} \Big|_{\bar{m}_1^3 \bar{m}_2^2} = \mathcal{C}_1 \cup \mathcal{C}_2 \cup \mathcal{C}_3, \quad (\text{C.2})$$

where:

$$\begin{aligned} \mathcal{C}_1 &= \text{Cut}_{[\ell, \ell - q_2]} \left[ \mathcal{M}_{5, \bar{m}_1^3}^{(0)}(\bar{p}_1; -\ell, \ell - q_2, k) \otimes_2 \mathcal{M}_{4, \bar{m}_2^2}^{(0)}(\bar{p}_2; \ell, -\ell + q_2) \right], \\ \mathcal{C}_2 &= \text{Cut}_{[\ell, \ell + q_1]} \left[ \mathcal{M}_{4, \bar{m}_1^3}^{(0)}(\bar{p}_1; -\ell, \ell + q_1) \otimes_2 \mathcal{M}_{5, \bar{m}_2^2}^{(0)}(\bar{p}_2; \ell, -\ell - q_1, k) \right], \\ \mathcal{C}_3 &= \text{Cut}_{[q_2]} \left[ \mathcal{M}_{4, \bar{m}_1^3}^{(1)}(\bar{p}_1; -q_2, k) \otimes_1 \mathcal{M}_{3, \bar{m}_2^2}^{(0)}(\bar{p}_2; q_2) \right]. \end{aligned} \quad (\text{C.3})$$

Tree-level contributions proportional to  $\bar{m}_1^3$  contain a localized matter propagator on line 1 and thus carry the overall factor  $\hat{\delta}(\ell \cdot \bar{u}_1)$ . Cut merging is required to avoid double counting terms with non-vanishing residues in more than one channel. In this case the merge is simple: using Bianchi identities (and trivial momentum relations) the tensor structures are rewritten into a basis where the overlap can be removed automatically. A convenient choice is the following set of six independent structures:

$$(\bar{u}_1 \cdot F_k \cdot \bar{u}_2)^2, \quad (q_1 \cdot F_k \cdot \bar{u}_1)^2, \quad (\ell \cdot F_k \cdot \bar{u}_1)^2, \quad (\bar{u}_1 \cdot F_k \cdot \bar{u}_2)(q_1 \cdot F_k \cdot \bar{u}_1), \quad (\bar{u}_1 \cdot F_k \cdot \bar{u}_2)(\ell \cdot F_k \cdot \bar{u}_1), \quad (q_1 \cdot F_k \cdot \bar{u}_1)(\ell \cdot F_k \cdot \bar{u}_1). \quad (\text{C.4})$$

A compact gauge-invariant representation of the complete one-loop waveform integrand is supplied in the ancillary file `integrand.m`.

We refer to Refs. [51, 52] for a detailed discussion of the cut-merging procedure. After performing a loop-momentum IBP reduction we verified that our merged integrand is compatible with that of Refs. [51, 52] up to terms polynomial in  $q_i^2$ , which give only contact (impact-parameter local) contributions and therefore drop out after the Fourier transform.

### Appendix D: Brown–Feynman–Passarino–Veltman reduction

We perform tensor reduction following the algorithm presented in Ref. [87]. The space of external momenta is spanned by the vectors  $v_i^\mu \in \{u_1^\mu, u_2^\mu, b^\mu, k^\mu\}$ . We define the projector,

$$P^{\mu\nu} = \sum_{i=1}^4 \hat{v}_i^\mu \hat{v}_i^\nu, \quad (\text{D.1})$$

where  $\hat{v}_i^\mu$  is the vector dual to  $v_i^\mu$ , *i.e.*  $v_i^\mu \hat{v}_{j\mu} = \delta_{ij}$ . A closed form of these vectors is given in terms of the Gram matrix  $G_{ij} = v_i \cdot v_j$  and its inverse:

$$\hat{v}_i^\mu = G_{ij}^{-1} v_j^\mu. \quad (\text{D.2})$$

As we work with four-dimensional external momenta, we have,

$$\eta^{\mu\nu} = P^{\mu\nu}, \quad (\text{D.3})$$

when contracted with an external momentum. For a generic tensor of rank  $N$ , we write,

$$T^{\mu_1 \dots \mu_N} = T_{\nu_1 \dots \nu_N} \prod_{i=1}^N P^{\mu_i \nu_i}. \quad (\text{D.4})$$

In particular, we have:

$$\begin{aligned} \Delta \hat{k}^\mu &= (w_2 \gamma - w_1) b^2 \bar{u}_1^\mu + (w_1 \gamma - w_2) b^2 \bar{u}_2^\mu + (1 - \gamma^2) b^2 k^\mu + (\gamma^2 - 1) b \cdot k b^\mu, \\ \Delta \hat{b}^\mu &= (w_1 - w_2 \gamma) b \cdot k \bar{u}_1^\mu + (w_2 - w_1 \gamma) b \cdot k \bar{u}_2^\mu + (\gamma^2 - 1) b \cdot k k^\mu - (w_1^2 - 2w_1 w_2 \gamma + w_2^2) b^\mu, \\ \Delta \hat{u}_1^\mu &= (w_2^2 (-b^2) - b \cdot k^2) \bar{u}_1^\mu + (\gamma b \cdot k^2 + w_1 w_2 b^2) \bar{u}_2^\mu + (w_2 \gamma - w_1) b^2 k^\mu + (w_1 - w_2 \gamma) b \cdot k b^\mu, \\ \Delta \hat{u}_2^\mu &= (\gamma b \cdot k^2 + w_1 w_2 b^2) \bar{u}_1^\mu + (w_1^2 (-b^2) - b \cdot k^2) \bar{u}_2^\mu + (w_1 \gamma - w_2) b^2 k^\mu + (w_2 - w_1 \gamma) b \cdot k b^\mu, \end{aligned} \quad (\text{D.5})$$

where

$$\Delta = \det G_{ij} = (\gamma^2 - 1) b \cdot k^2 - (w_1^2 - 2w_1 w_2 \gamma + w_2^2) b^2. \quad (\text{D.6})$$

### Appendix E: Loop Integrals

All one-loop integrals we need belong to the same integral family, characterized by a single cut on a matter line imposed by the classical limit. When the cut is imposed on  $\bar{u}_1$ , the integral family is defined by,

$$I_{1, a_2, a_3, a_4, a_5}^{[1]} := - \int_{\hat{\ell}} \frac{i\pi \delta(D_{o:1})}{(D_{o:2} + \alpha \varepsilon)^{a_2} D_{o:3}^{a_3} D_{o:4}^{a_4} D_{o:5}^{a_5}}, \quad (\text{E.1})$$

where the invariants are,

$$D_{o:1} = \bar{u}_1 \cdot \ell, \quad D_{o:2} = \bar{u}_2 \cdot \ell, \quad D_{o:3} = \ell^2, \quad D_{o:4} = (\ell + q_1)^2, \quad D_{o:5} = (\ell - q_2)^2. \quad (\text{E.2})$$

The expression  $1/(D_{o:2} + i\alpha \varepsilon)^{a_2}$  should be understood as a distribution, defined as the  $(a_2 - 1)$ -th derivative of the simple pole with an  $i\varepsilon$  prescription (when  $\alpha = 1$ ) or via a principal value prescription ( $\alpha = 0$ ):

$$\frac{1}{(D_{o:2} + i\alpha \varepsilon)^{a_2}} = \frac{(-1)^{n-1}}{(n-1)!} \partial D_{o:2}^{n-1} \left( \frac{1}{D_{o:2} + i\alpha \varepsilon} \right), \quad (\text{E.3})$$

where for  $a_2 = 1$ , we define,

$$\frac{1}{D_2 + i\alpha \varepsilon} = \mathcal{P} \left( \frac{1}{D_{o:2}} \right) - i\alpha \pi \delta(D_{o:2}). \quad (\text{E.4})$$

We denote the principal value by  $\mathcal{P}(1/D_{o:2})$ . We thus have,

$$\frac{1}{(D_{o:2} + i\alpha \varepsilon)^n} = \mathcal{P} \left( \frac{1}{D_{o:2}^n} \right) - i\alpha \pi \frac{(-1)^{n-1}}{(n-1)!} \delta^{(n-1)}(D_{o:2}), \quad (\text{E.5})$$

where  $\delta^{(r)}$  denotes the  $r^{\text{th}}$  derivative of the Dirac delta distribution.

Using IBPs and the method of canonical DEs as in Refs. [1, 54, 55], we find 10 MIs, whose analytic expressions up to the relevant order in  $\epsilon$  is,

$$\begin{aligned}
I_{1,0,0,1,0}^{[1]} &= -\frac{w_1}{8\pi} [1 + (i\pi + \log(\pi) + 2 - 2\log(w_1))\epsilon] + \mathcal{O}(\epsilon^2), \\
I_{1,0,1,0,1}^{[1]} &= -\frac{i}{16\sqrt{-q_1^2}} + \mathcal{O}(\epsilon), \\
I_{1,0,1,1,0}^{[1]} &= \frac{-i\pi + 2\log(w_1 + \sqrt{w_1^2 - q_2^2}/\sqrt{-q_2^2})}{16\pi\sqrt{w_1^2 - q_2^2}} + \mathcal{O}(\epsilon), \\
I_{1,0,1,1,1}^{[1]} &= \frac{1}{32\pi(-q_1^2)w_1\epsilon} + \frac{i\pi + 2\log(q_2^2/q_1^2) - 2\log w_1 + \log \pi}{32\pi(-q_1^2)w_1} + \mathcal{O}(\epsilon), \\
I_{1,1,0,0,1}^{[1]} &= \frac{\alpha}{16\pi\sqrt{\gamma^2 - 1}\epsilon} + \frac{-i\pi + \alpha[\log(\gamma^2 - 1) - 2\log w_2 + \log(4\pi)]}{16\pi\sqrt{\gamma^2 - 1}} + \mathcal{O}(\epsilon), \\
I_{1,1,0,1,0}^{[1]} &= \frac{\alpha}{16\pi\sqrt{\gamma^2 - 1}\epsilon} + \frac{-i\pi + 2\log(\gamma + \sqrt{\gamma^2 - 1}) + \alpha[\log(\gamma^2 - 1) - 2\log w_1 + \log(4\pi)]}{16\pi\sqrt{\gamma^2 - 1}} + \mathcal{O}(\epsilon), \\
I_{1,1,0,1,1}^{[1]} &= \frac{1}{32\pi w_1 w_2 \epsilon} + \frac{i\pi - 2\log w_2 + \log \pi - 2\alpha \log(\gamma + \sqrt{\gamma^2 - 1})}{32\pi w_1 w_2} + \mathcal{O}(\epsilon), \\
I_{1,1,1,0,1}^{[1]} &= \frac{\alpha}{16\pi(-q_1^2)\sqrt{\gamma^2 - 1}\epsilon} + \frac{i\pi + \alpha[2\log(w_2) - 2\log(-q_1^2) - \log(\gamma^2 - 1) + \log(4\pi)]}{16\pi(-q_1^2)\sqrt{\gamma^2 - 1}} + \mathcal{O}(\epsilon), \\
I_{1,1,1,1,0}^{[1]} &= \frac{\alpha}{16\pi(-q_2^2)\sqrt{\gamma^2 - 1}\epsilon} \\
&\quad + \frac{i\pi - 2\log(\gamma + \sqrt{\gamma^2 - 1}) + \alpha[2\log(w_1) - 2\log(-q_2^2) - \log(\gamma^2 - 1) + \log(4\pi)]}{16\pi(-q_2^2)\sqrt{\gamma^2 - 1}} + \mathcal{O}(\epsilon).
\end{aligned} \tag{E.6}$$

The parameter  $\alpha$  again specifies the  $i\epsilon$  prescription for the propagator: here,  $\alpha = 0$  corresponds to the principal-value prescription for the massive propagator, while  $\alpha = -1$  corresponds to the retarded prescription.

The pentagon integral through  $\mathcal{O}(\epsilon^0)$  can be written as a linear combination of four-point functions given above,

$$\begin{aligned}
I_{1,1,1,1,1}^{[1]} &= \frac{1}{2[(q_1^2)^2 w_1^2 - 2q_1^2 q_2^2 w_1 w_2 \gamma + (q_2^2)^2 w_2^2]} \\
&\quad \times \left[ 2(-q_1^2 w_1 \gamma (q_1^2 - q_2^2) + q_2^2 w_2 (q_1^2 - q_2^2) - 2q_1^2 w_1^2 w_2) I_{1,0,1,1,1}^{[1]} \right. \\
&\quad - 2(w_1^2 (-q_1^2 + 2w_2^2) + w_1 w_2 \gamma (q_1^2 + q_2^2) - q_2^2 w_2^2) I_{1,1,0,1,1}^{[1]} \\
&\quad + ((q_1^2)^2 - q_1^2 \gamma^2 (q_1^2 - q_2^2) - q_1^2 q_2^2 + 2q_2^2 w_2^2 - 2q_1^2 w_1 w_2 \gamma) I_{1,1,1,1,0}^{[1]} \\
&\quad \left. + ((q_2^2)^2 + q_2^2 \gamma^2 (q_1^2 - q_2^2) - q_1^2 q_2^2 + 2q_1^2 w_1^2 - 2q_2^2 w_1 w_2 \gamma) I_{1,1,1,0,1}^{[1]} \right] + \mathcal{O}(\epsilon).
\end{aligned} \tag{E.7}$$

Similarly  $I_{a_1,1,a_3,a_4,a_5}^{[2]}$  is defined with a matter cut on the leg carrying  $\bar{u}_2$ .

## Appendix F: Fourier Transform Details

In this Appendix, we provide details of our method for computing the Fourier transform of Feynman integrals. We will discuss three different methods: using contour deformation; using Schwinger parametrization; and resumming the post-Newtonian expansion. The first method has the widest range of applicability to the integrals of interest. We have found the other two useful for some of the integrals and as a cross-check.

*a. Contour deformation* We illustrate the general approach by carrying out the Fourier transform in two examples:

$$\begin{aligned}
f_1(w_1, w_2, \gamma, b \cdot k, b^2) &= - \int \hat{d}^D q \hat{\delta}(2\bar{p}_1 \cdot q) \hat{\delta}(2\bar{p}_2 \cdot (k - q)) e^{ib \cdot q} \frac{\log(-q^2/\mu^2)}{(k - q)^2}, \\
f_2(w_1, w_2, \gamma, b \cdot k, b^2) &= - \int \hat{d}^D q \hat{\delta}(2\bar{p}_1 \cdot q) \hat{\delta}(2\bar{p}_2 \cdot (k - q)) e^{ib \cdot q} \frac{\log(-q^2/\mu^2)}{q^2}.
\end{aligned} \tag{F.1}$$

All the essential features can be understood in these examples. We begin by choosing a convenient parametrization for  $q$  in terms of the external momenta [1, 50],

$$q^\mu = z_1 \bar{u}_1^\mu + z_2 \bar{u}_2^\mu + z_b \frac{b^\mu}{b} + z_v \tilde{v}_\perp^\mu, \quad (\text{F.2})$$

where  $v_\perp^\mu$  is a unit vector orthogonal to  $u_1^\mu$ ,  $u_2^\mu$  and  $b^\mu$ :

$$v_\perp^2 = -1, \quad v_\perp \cdot b = v_\perp \cdot u_1 = v_\perp \cdot u_2 = 0. \quad (\text{F.3})$$

As we are restricting to four-dimensional kinematics, the contraction of this vector with  $k^\mu$  is also simple,

$$(k \cdot v_\perp)^2 = -(\hat{w}_1^2 - 2\hat{w}_1\hat{w}_2\gamma + \hat{w}_2^2) + \frac{(b \cdot k)^2}{b^2} = \frac{\Delta}{b^2(\gamma^2 - 1)}, \quad (\text{F.4})$$

where  $\Delta$  is given in Eq. (D.6), and we define,

$$\hat{w}_i = \frac{w_i}{\sqrt{\gamma^2 - 1}}. \quad (\text{F.5})$$

For generic  $D$ , the measure reads

$$\hat{d}^D q \hat{\delta}(2\bar{p}_1 \cdot q_1) \hat{\delta}(2\bar{p}_2 \cdot (k - q)) = d^4 z d^{D-4} v_\perp \frac{\sqrt{\gamma^2 - 1} z_v^{D-4}}{4(2\pi)^{D-2} \bar{m}_1 \bar{m}_2} \delta(z_1 + \gamma z_2) \delta(z_2(\gamma^2 - 1) + w_2), \quad (\text{F.6})$$

where the integration over  $z_v$  is along the positive real axis and  $d^{D-4} v_\perp$  is a  $(D-4)$ -dimensional spherical integral. In  $D = 4$ , we recover the parametrization presented in Ref. [50],

$$v_\perp^\mu = \frac{\epsilon^{\mu\nu\rho\sigma} u_{1\nu} u_{2\rho} b_\sigma}{\sqrt{\gamma^2 - 1} b}, \quad (\text{F.7})$$

and the  $z_v$  integration runs along the whole real axis. For the finite part of the amplitude, the integration in  $D = 4$  suffices. Here, we find,

$$f_i(w_1, w_2, \gamma, b \cdot k, b^2) = \frac{1}{16\pi^2 \bar{m}_1 \bar{m}_2 \sqrt{\gamma^2 - 1}} \int_{-\infty}^{+\infty} dz_b \int_{-\infty}^{\infty} dz_v F_i(z_b, z_v), \quad (\text{F.8})$$

where,

$$F_1(z_b, z_v) = \frac{e^{-ibz_b} \log(z_v^2 + z_b^2 + \hat{w}_2^2)}{(z_v + k \cdot v_\perp)^2 + (z_b + b \cdot k/b)^2 + \hat{w}_1^2}, \quad (\text{F.9})$$

$$F_2(z_b, z_v) = \frac{e^{-ibz_b} \log(z_v^2 + z_b^2 + \hat{w}_2^2)}{z_v^2 + z_b^2 + \hat{w}_2^2}.$$

In general, we expect to find four poles and four branch points of the integrand in the complex  $z_v$  plane (see Fig. 13), corresponding to singularities at  $q_{1,2}^2 = 0$ . In the  $z_v$  plane, these singularities will be found at,

$$\hat{z}_1^\pm = \pm i \sqrt{z_b^2 + \hat{w}_2^2}, \quad \hat{z}_2^\pm = -k \cdot v_\perp \pm i \left[ \left( z_b + \frac{b \cdot k}{b} \right)^2 + \hat{w}_1^2 \right]^{1/2}. \quad (\text{F.10})$$

In the specific cases under consideration, the first integrand  $F_1$  has a pole at  $q_2^2 = 0$  and a branch cut starting at  $q_1^2 = 0$ , whereas the second integrand  $F_2$  has a pole overlapping with a branch cut at  $q_1^2 = 0$ .

We apply Cauchy's theorem to deform the integration contour and encircle the singularities either in the upper- or lower-half planes (UHP and LHP, respectively). The contour must be considered carefully, as the integration along the discontinuity is divergent whenever the branch points merge with poles. Accordingly, we need to split the contour into two pieces, as shown in Fig. 13:

- A (small) circular contour with radius  $\rho$  nearly encircling the pole (and possibly branch point) and ending on the two sides of the branch cut.

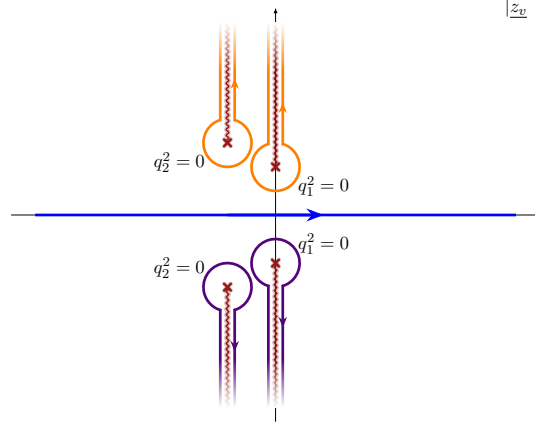


FIG. 13. The analytic structure of the  $z_v$  integrals. In general each integral has four singularities corresponding to the configurations in which  $q_1^2 = 0$  and  $q_2^2 = 0$ . We may choose a representation of the function so that all the branch cuts are parallel to the imaginary axis. We can apply Cauchy's residue theorem to deform the integration contour in the upper- or lower-half plane to encircle the singularities.

- The integration over the discontinuity from a distance  $\rho$  from the singularity to infinity along the pure imaginary direction (corresponding to our choice of branch cuts). For this contribution we change integration variable from  $z_v$  to  $x$  via  $z_v = \hat{z}_{1,2}^+ + ix + i\rho$ .

If we have a pole and branch point which merge, the integrals along the two contours are separately divergent as  $\rho \rightarrow 0$ , but the sum of the two integrals is finite. The discontinuity integral of interest can be written as the integration of a rational function on a line. We can rewrite the integral of a rational function  $R(x)$  along a path between two complex points  $a$  and  $b$  as a contour integral of the function  $R(x) \log\left(\frac{x-a}{x-b}\right)$ , with a branch cut along a path from  $a$  to  $b$ . We can then evaluate the integral using Cauchy's residue theorem,

$$\begin{aligned} \int_a^b dx R(x) &= -\frac{1}{2\pi i} \int_{\gamma} dx R(x) \log\left(\frac{x-a}{x-b}\right) \\ &= -\sum_i \text{Res}_{x=z_i} R(x) \log\left(\frac{x-a}{x-b}\right), \end{aligned} \quad (\text{F.11})$$

where  $\gamma$  is a positively oriented contour encircling the branch cut from  $a$  to  $b$  and  $\{z_i\}$  are the poles of  $R(x)$  in the complex plane. If  $R(x)$  also contains square roots, we must first rationalize the integrand (for this purpose, we used the *Mathematica* package `RationalizeRoots` [105]). It may happen that the discontinuity contribution has integrable singularities along the integration path (see for example, Eq. (F.35)). Should this happen, we must split the integration contour, and apply the rewriting technique piecewise.

For the first integral, the  $z_v$  integration reads,

$$\begin{aligned} \int_{-\infty}^{\infty} dz_v F_1(z_b, z_v) &= \int_{\mathcal{O}_{\rho}[\hat{z}_2^+]} dz_v F_1(z_b, z_v) + i \int_0^{\infty} dx \text{Disc}_{\hat{z}_1^+ > 0} F_1(z_b, z_v) \\ &= \frac{\pi \log \left[ \left( \sqrt{(z_b + b \cdot k/b)^2 + \hat{w}_1^2} + \sqrt{z_b^2 + \hat{w}_2^2} \right)^2 - (b \cdot k)^2/b^2 \right]}{\sqrt{(z_b + b \cdot k/b)^2 + \hat{w}_1^2}}, \end{aligned} \quad (\text{F.12})$$

while for the second integral we find,

$$\begin{aligned} \int_{-\infty}^{\infty} dz_v F_2(z_b, z_v) &= \int_{\mathcal{O}_{\rho}[\hat{z}_1^+]} dz_v F_2(z_b, z_v) + i \int_{\rho}^{\infty} dx \text{Disc}_{\hat{z}_1^+ > 0} F_2(z_b, z_v) \\ &= \frac{2\pi \log(2\sqrt{z_b^2 + \hat{w}_2^2})}{\sqrt{z_b^2 + \hat{w}_2^2}}. \end{aligned} \quad (\text{F.13})$$

In the second integration we needed to keep the cut-off in  $\rho$  explicit as the two contributions diverge separately as  $\log \rho$ . The divergence cancels in the sum.

At this point, we are left with a one-dimensional Fourier transform. For waveform contributions up to one-loop order, the integrand will involve square roots and logarithms with nested square roots. In the complex plane, the singularities in  $z_b$  are located at,

$$z_b = \pm i\hat{w}_2, \quad z_b = -\frac{b \cdot k}{b} \pm i\hat{w}_1. \quad (\text{F.14})$$

We choose a representation of the function such that all branch cuts are parallel to the imaginary axis. The integration over  $z_b$  can then be performed numerically efficiently by contour deformation. We deform the contour in the lower-half plane to encircle the singularities so that  $e^{-ibz_b}$  gives an exponential suppression at large  $|z_b|$ . This allows for a numerically stable and efficient integration strategy.

We can also aim at a fully analytic evaluation of the waveform integrals in the time domain. Jakobsen *et al.* already showed at tree-level [45] that the one-dimensional Fourier transform in  $z_b$  can be bypassed by combining it with the Fourier transform from frequency to the time domain (for a detailed discussion, see also Refs. [46, 52]). At one-loop, such a simplification persists, though not to the same extent. Together with the trivial delta function and derivatives thereof, we would find an extra integration with an extra principal-value extraction or logarithmic ‘propagator’, instead of the exponential factor. Then, even though the space of functions reduces to a familiar class (*e.g.* polylogarithms and square roots), the result becomes harder to handle analytically. We did not pursue this direction.

The contour-integration method is tailored for the one-loop waveform computation as the loop integrals involve at most logarithms and square roots. However, it is unlikely to be an optimal approach for higher-order computations. We expect that a more unified treatment of Fourier and loop integrals will be needed to compute the required integrals efficiently.

*b. Schwinger parametrization* An alternative integration method for integrals of the form,

$$S_{\alpha_1, \alpha_2} = \int \hat{d}^D q \hat{\delta}(2\bar{p}_1 \cdot q) \hat{\delta}(2\bar{p}_2 \cdot (k - q)) \frac{e^{ib \cdot q}}{(-q^2)^{\alpha_1} [-(k - q)^2]^{\alpha_2}}, \quad (\text{F.15})$$

is a generalization of the Schwinger-parametrization approach introduced by Vernizzi and Riva [106]. We can rewrite,

$$\frac{e^{ib \cdot q}}{(-q^2)^{\alpha_1} [-(k - q)^2]^{\alpha_2}} = \frac{1}{\Gamma(\alpha_1)\Gamma(\alpha_2)} \int_0^\infty dx_1 x_1^{\alpha_1-1} \int_0^\infty dx_2 x_2^{\alpha_2-1} e^{ib \cdot q + x_1 q^2 + x_2 (k - q)^2}. \quad (\text{F.16})$$

Parametrize the  $q$  integration as described in the previous subsection and notice that the  $z_b$  integral is now a simple Gaussian integration,

$$S_{\alpha_1, \alpha_2} = \frac{(2\pi)^{2-d} \sqrt{\pi}}{4\bar{m}_1 \bar{m}_2 \sqrt{\gamma^2 - 1} \Gamma(\alpha_1) \Gamma(\alpha_2)} \int d^2 x \frac{x_1^{\alpha_1-1} x_2^{\alpha_2-1}}{\sqrt{x_1 + x_2}} \exp \left[ -\hat{w}_2^2 (x_1 - x_2) - 2\hat{w}_1 \hat{w}_2 \gamma x_2 + \frac{i\mathbf{b} + 2x_2 b \cdot k/b}{4(x_1 + x_2)} \right] \times \int dz_v z_v^{D-4} e^{-(x_1+x_2)z_v^2} \int d^{D-4} v_\perp e^{-2x_2 z_v k \cdot v_\perp}. \quad (\text{F.17})$$

First, perform the angular integration

$$\begin{aligned} \int d^{D-4} v_\perp e^{-2x_2 z_v k \cdot v_\perp} &= \frac{2\pi^{(D-4)/2}}{\Gamma(\frac{D-4}{2})} \int_{-1}^{+1} d \cos \theta \sin^{(D-6)/2} \theta \exp \left[ 2x_2 z_v \cos \theta \sqrt{\frac{\Delta}{b^2(\gamma^2 - 1)}} \right] \\ &= 2\pi^{(D-3)/2} \left[ 2x_2 z_v \sqrt{\frac{\Delta}{2b^2(\gamma^2 - 1)}} \right]^{(5-D)/2} I_{(D-5)/2} \left( 2x_2 z_v \sqrt{\frac{\Delta}{b^2(\gamma^2 - 1)}} \right) \\ &\stackrel{D=4}{=} 2 \cosh \left( 2x_2 z_v \sqrt{\frac{\Delta}{b^2(\gamma^2 - 1)}} \right), \end{aligned} \quad (\text{F.18})$$

where  $I_\alpha(x)$  is a modified Bessel function of the first kind. In the first line, we split the angular integration into two: a direction which is longitudinal to  $k^\mu$ , whose projection is fixed in Eq. (F.4), and an additional angular integration which factorizes. Note that the sign in front of the square root in the exponent is irrelevant. As we take the limit  $D \rightarrow 4$ , we recover the sum of two exponentials, with exponents which differ by a sign, *i.e.* we recover the  $z_v$  integration along the full real axis. The  $z_v$  integration is a known integral:

$$\int_0^\infty dz_v e^{-\alpha z_v^2} z_v^{(D-3)/2} I_{(D-5)/2}(z_v) = e^{1/\alpha} (2\alpha)^{(3-D)/2}. \quad (\text{F.19})$$

The full result then takes the form,

$$S_{\alpha_1, \alpha_2} = \frac{(4\pi)^{1-D/2}}{4\bar{m}_1\bar{m}_2\sqrt{\gamma^2-1}\Gamma(\alpha_1)\Gamma(\alpha_2)} \int d^2x \frac{x_1^{\alpha_1-1}x_2^{\alpha_2-1}}{(x_1+x_2)^{D/2-1}} \exp\left[-\frac{x_1^2\hat{w}_2^2+x_2^2\hat{w}_1^2+2x_1x_2\hat{w}_1\hat{w}_2\gamma-b^2/4-ix_2b\cdot k}{(x_1+x_2)}\right]. \quad (\text{F.20})$$

Finally, we perform the change of variables suggested in Ref. [106]:

$$x_1 = -\frac{b^2(1-x)}{4\lambda}, \quad x_2 = -\frac{b^2x}{4\lambda}, \quad (\text{F.21})$$

and recognize the following integral representation of the modified Bessel function of the second kind:

$$\int_0^\infty d\lambda e^{-a/\lambda-\lambda}\lambda^b = 2a^{(b+1)/2}K_{-1-b}(2\sqrt{a}). \quad (\text{F.22})$$

The final result for  $S$  is,

$$S_{\alpha_1, \alpha_2} = \frac{(4\pi)^{1-D/2}(\mathbf{b}/2)^{\alpha_1+\alpha_2+1-D/2}}{2\bar{m}_1\bar{m}_2\sqrt{\gamma^2-1}\Gamma(\alpha_1)\Gamma(\alpha_2)} \int_0^1 dx e^{ixb\cdot k} (1-x)^{\alpha_1-1}x^{\alpha_2-1}\Omega(x)^{D/2-\alpha_1-\alpha_2-1}K_{\alpha_1+\alpha_2+1-D/2}(\mathbf{b}\Omega(x)), \quad (\text{F.23})$$

in which,

$$\Omega(x) = \sqrt{x^2\hat{w}_1^2+(1-x)^2\hat{w}_2^2+2(1-x)x\hat{w}_1\hat{w}_2\gamma}. \quad (\text{F.24})$$

We observe that most of the Fourier-loop CMIs can be written in this form. Indeed, the Fourier transforms of all the loop MIs except  $j_{1,0,1,0,1}^{L,(1)}$  and  $j_{1,1,1,1,1}^{L,(1)}$  can be written in this form; see Ref. [1]. The cases  $\alpha_1 = 0$  or  $\alpha_2 = 0$  cannot be obtained trivially from the representation (F.23), but a parallel yet simpler derivations gives,

$$\begin{aligned} S_{\alpha,0} &= \frac{(4\pi)^{1-D/2}(2\hat{w}_2/\mathbf{b})^{D/2-(\alpha+1)}}{2\bar{m}_1\bar{m}_2\sqrt{\gamma^2-1}\Gamma(\alpha)} K_{\alpha+1-D/2}(\mathbf{b}\hat{w}_2), \\ S_{0,\alpha} &= \frac{(4\pi)^{1-D/2}(2\hat{w}_1/\mathbf{b})^{D/2-(\alpha+1)}}{2\bar{m}_1\bar{m}_2\sqrt{\gamma^2-1}\Gamma(\alpha)} e^{ib\cdot k} K_{\alpha+1-D/2}(\mathbf{b}\hat{w}_1). \end{aligned} \quad (\text{F.25})$$

*c. Tree-level integrals to  $\mathcal{O}(\epsilon)$*  In this paragraph, we continue our consideration of the integrals in the family (F.15). In principle, we can expand the results (F.23,F.25) around  $D = 4$  to obtain the  $\epsilon$  contributions to the Fourier integrals, as the divergent contributions are always proportional to the tree-level waveform. We can write the latter in terms of the integrals  $S_{1,0}$ ,  $S_{0,1}$  and  $S_{1,1}$ , along with their derivatives with respect to  $\mathbf{b}$ . On the other hand, it is useful to avoid the appearance of Bessel functions, and write these terms as a one-dimensional Fourier transform just of logarithms. We start from the  $D$ -dimensional parametrization of the integration (F.6), without assuming any particular form of the orthogonal vector  $v_\perp^\mu$  spanning the  $(D-3)$ -dimensional space orthogonal to the scattering plane. We can further split the angular integration,

$$v_\perp^\mu = z\sqrt{\frac{\Delta}{-b^2(\gamma^2-1)}}\hat{k}^\mu + \sqrt{1-z^2}\hat{v}_\perp^\mu, \quad (\text{F.26})$$

where  $\hat{k}^\mu$  is the dual vector associated to  $k^\mu$ , defined in Eq. (D.5), and  $\hat{v}_\perp^\mu$  is a unit vector orthogonal to the four-dimensional physical space. The integration over the  $(D-4)$ -dimensional angle factorizes to yield,

$$\int d^{D-5}\hat{v}_\perp = \frac{2\pi^{D/2-2}}{\Gamma(\frac{D}{2}-2)}. \quad (\text{F.27})$$

The full integrals are then,

$$S_{\alpha_1, \alpha_2} = \frac{2}{(4\pi)^{D/2}\Gamma(\frac{D}{2}-2)\sqrt{\gamma^2-1}\bar{m}_1\bar{m}_2} \int_{-\infty}^{+\infty} dz_b e^{-ibz_b} \int_0^\infty dz_v z_v^{D-4} \int_{-1}^{+1} dz (1-z^2)^{D/2-3} F_{\alpha_1, \alpha_2}(z_b, z_v, z), \quad (\text{F.28})$$

in which,

$$F_{\alpha_1, \alpha_2}(z_b, z_v, z) = \frac{1}{(z_b^2+z_v^2+\hat{w}_2^2)^{\alpha_1} \left[ (z_b+b\cdot k/\mathbf{b})^2+z_v^2+2z_bz_v\sqrt{\frac{\Delta}{(-b^2)(\gamma^2-1)}} + \frac{\Delta}{(-b^2)(\gamma^2-1)} + \hat{w}_1^2 \right]^{\alpha_2}}. \quad (\text{F.29})$$

The  $z$  integration can be computed in terms of an  ${}_2F_1$  hypergeometric function, which we can then expand for small  $\epsilon$ . We then need to perform the  $z_v$  integral analytically. As we already know the analytic results for the cases in which only one of the two denominators appear, we can focus on the remaining case,  $(\alpha_1, \alpha_2) = (1, 1)$ . The  $z_v$  integration can be computed in terms of dilogarithms and logarithms (possibly squared), using a strategy similar to the one presented above.

*d. Resummed small-velocity expansion* We present last an additional strategy that has proven particularly useful in finding a compact result for the Fourier transform of  $j_{1,0,1,0,1}^{L,\hat{u}_1}$  in terms of a Struve-H function:

$$\begin{aligned} \tilde{S} &= e^{ib \cdot k} \int \hat{d}^4 q \hat{\delta}(2\bar{p}_1 \cdot (k - q)) \hat{\delta}(2\bar{p}_2 \cdot q) e^{-ib \cdot q} \frac{2 \log((w_1 + \sqrt{w_1^2 - q^2})/\sqrt{-q^2}) - i\pi}{16\pi\sqrt{w_1^2 - q^2}} \\ &= e^{ib \cdot k} \int \hat{d}^4 q \hat{\delta}(2\bar{p}_1 \cdot (k - q)) \hat{\delta}(2\bar{p}_2 \cdot q) e^{-ib \cdot q} \left[ -i \sum_{n=0}^{\infty} \frac{\left(\frac{1}{2}\right)_n}{16n! \sqrt{-q^2}} \left(\frac{w_1^2}{q^2}\right)^n - \sum_{n=0}^{\infty} \frac{n! w_1}{8\pi \left(\frac{3}{2}\right)_n q^2} \left(\frac{w_1^2}{q^2}\right)^n \right]. \end{aligned} \quad (\text{F.30})$$

In these expressions,  $(a)_n$  denotes the Pochhammer symbol,  $(a)_n = \Gamma(n + a)/\Gamma(a)$ . Each term in the sums is within the integral families of Eq. (F.25):

$$\tilde{S} = \frac{\sqrt{\pi} e^{ib \cdot k}}{4\bar{m}_1 \bar{m}_2 (4\pi)^2 \mathbf{b}} \sum_{n=0}^{\infty} (1 - \gamma^2)^n \left(\frac{\hat{w}_1 \mathbf{b}}{2}\right)^{n+1} \left[ -\frac{\sqrt{2}i K_{n-\frac{1}{2}}(\hat{w}_1 \mathbf{b})}{n! \sqrt{(\gamma^2 - 1)\hat{w}_1 \mathbf{b}}} + \frac{K_n(\hat{w}_1 \mathbf{b})}{\Gamma(n + \frac{3}{2})} \right]. \quad (\text{F.31})$$

The first series of terms can be resummed into a simple exponential. In the second term in the sum, we substitute the following integral representation of the Bessel function,

$$K_n(z) = \frac{\sqrt{\pi} z^n}{2^n \Gamma(n + \frac{1}{2})} \int_1^{\infty} dt e^{-tz} (t^2 - 1)^{n-1/2}. \quad (\text{F.32})$$

Upon exchanging the order of integration and summation, we can recognize the expansion of a Struve function,

$$\mathbf{H}_{-1}(z) = \sum_{n=0}^{\infty} \frac{\left(\frac{z}{2}\right)^{2n}}{\Gamma(n + \frac{3}{2}) \Gamma(n + \frac{1}{2})}. \quad (\text{F.33})$$

Finally, using the change of variables  $t = \cosh x$ , we obtain the result,

$$\tilde{S} = \frac{e^{ib \cdot k}}{128\pi \bar{m}_1 \bar{m}_2} \left[ \int_0^{\infty} dx e^{-\hat{w}_1 \mathbf{b} \cosh x} \hat{w}_1 \mathbf{H}_{-1}(w_1 \mathbf{b} \sinh x) - i \frac{e^{-\hat{w}_1 \mathbf{b} \gamma}}{\mathbf{b} \sqrt{\gamma^2 - 1}} \right], \quad (\text{F.34})$$

where the representation of the second term is particularly well-suited to numerical evaluation thanks to the double-exponential suppression for  $x \gtrsim 0$ . We can compare this result with the contour deformation strategy. We notice that along  $q^2 > 0$ , the discontinuity of the triangle integral takes a discontinuous form,

$$\text{Disc}_{q^2 > 0} \frac{2 \log((w_1 + \sqrt{w_1^2 - q^2})/\sqrt{-q^2}) - i\pi}{16\pi\sqrt{w_1^2 - q^2}} = \begin{cases} -\frac{i}{8\sqrt{w_1^2 - q^2}}, & 0 < q^2 < w_1^2 \\ -\frac{1}{8\sqrt{q^2 - w_1^2}}, & q^2 > w_1^2 \end{cases}. \quad (\text{F.35})$$

The integration in  $z_v$  along the discontinuity of these expressions yields the same splitting presented in Eq. (F.34)<sup>8</sup>. In particular, one obtains,

$$\begin{aligned} \tilde{S} &= \frac{e^{ib \cdot k}}{16\pi^2 \bar{m}_1 \bar{m}_2} \int_{-\infty}^{+\infty} dz_b e^{iz_b \mathbf{b}} \left[ \frac{1}{8} \arcsin \frac{w_1}{\sqrt{z_b^2 + \hat{w}_1^2 \gamma^2}} + \frac{i}{16} \log(z_b^2 + \hat{w}_1^2 \gamma^2) \right] \\ &= \frac{e^{ib \cdot k}}{128\pi \bar{m}_1 \bar{m}_2 \sqrt{\gamma^2 - 1}} \left[ \frac{1}{\pi} \int_{-\infty}^{+\infty} dz_b e^{iz_b \mathbf{b}} \arcsin \frac{w_1}{\sqrt{z_b^2 + \hat{w}_1^2 \gamma^2}} - i \frac{e^{-\hat{w}_1 \mathbf{b} \gamma}}{\mathbf{b}} \right], \end{aligned} \quad (\text{F.36})$$

where the two terms are ordered accordingly to the splitting in Eq. (F.35). The result matches the small-velocity-resummed result (F.34) numerically.

<sup>8</sup> The  $z_v$  integration of the second expression does not converge. We may, however, observe, that with the use of any regulator (for example,  $z_v^{-\rho}$  or, equivalently performing the Fourier integral in

dimensional regularization), the divergent part as we remove the regulator yields a result polynomial in  $z_b$  — ultimately integrating to a localized contribution in impact parameter space which we drop.